Sigma J Eng Nat Sci, Vol. 43, No. 5, pp. 1760–1784, October, 2025

Sigma Journal of Engineering and Natural Sciences
Web page info: https://sigma.yildiz.edu.tr
DOI: 10.14744/sigma.2025.00054

Research Article

Electrokinetic effect on flow of two-phase fluid in a circular tube

Sangeetha J[1,*], Ponalagusamy R[1]

[1]*Department of Mathematics, National Institute of Technology, Tiruchirappalli, Tamil Nadu, 620015, India*

ARTICLE INFO

Article history
Received: 29 February 2024
Revised: 12 June 2024
Accepted: 24 September 2024

Keywords:
Electric Field; K-L Fluid; Newtonian Fluid, Two-Phase Model, Wall Shear Stress

ABSTRACT

In this article, we investigated the steady-state motion of two-phase immiscible fluids through a rigid wall tube. The fluid confined in the mid-region is represented as Kuang-Luo (K-L) fluid and the outer, region is occupied by Newtonian fluid. Both the fluid is considered as an electrically conducting fluid and the fluid undergoes the electroosmotic effect when an electric field is applied to it, externally. Based on the circumstances, with an appropriate boundary condition the analytical formulation for the velocity profiles of the fluid, flow flux, motion in the plug core region, plug core radius and wall shear stress was done. The numerical analysis of simulation effects was made on the K-L parameters, electro-osmotic effect and yield stress. This case study reveals the fact that whenever the K-L parameter (θ_2) and the yield stress(τ_0) increases, the velocity profiles of the fluid decrease and the opposite behaviour is identified by increasing the electrokinetic term and K-L parameter (θ_1) found in dealing with the wall shear stress properties. The significance of formulating the K-L constitutive equation using an empirical formula obtained from the experimental values of apparent viscosity, shear rate and yield stress of the human and canine blood samples provides the best approximate result. Aspired from this accuracy, the model has been constructed and analysed with appreciable values under the external electric field in the rigid circular conduit and the graphical results were displayed. A comparison of the various existing models with the present model was made and the applicability of the prescribed model provides a generalized case of non-Newtonian fluids like Casson fluid, Bingham Fluid and Newtonian fluid. Additionally, an analysis of the proposed mathematical model's significance on physiological applications has been discussed. For the first time, it is reported that for any value of the yield stress, the flow of two-phase immiscible fluids exhibits a realistic flow phenomenon when $\theta_1 \leq \theta_2$. The coarse-grained consequential amount of declined percentage has been seen from the two-layered Newtonian-Newtonian model is approximately higher than the Casson-Newtonian (6.74%), Bingham-Newtonian (17.92%) and K-L-Newtonian (22.77%) in velocity profiles. In the absence of an electric field ($U_e = 0$), Casson fluid is approximately 1.02% higher than the presence of an electric field ($U_e = 0.5$) while dealing with wall shear stress and similarly for the K-L model ($U_e = 0$) is appropriately greater than 0.078 % for $U_e = 0.5$. The pressure drop (Δp) for the K-L parameter $\theta_1 = 0.1, 0.2$ is approximately 0.21 % higher than the $\theta_1 = 0.3$ for the fixed viscosity index $\theta_2 = 0.3$. The results of the prescribed model are highly beneficial for simulating electrically conductive lubricants as applications of the engineering field.

Cite this article as: Sangeetha J, Ponalagusamy R. Electrokinetic effect on flow of two-phase fluid in a circular tube. Sigma J Eng Nat Sci 2025;43(5):1760–1784.

***Corresponding author.**
*E-mail address: sangeethajagan009@gmail.com

This paper was recommended for publication in revised form by Editor-in-Chief Ahmet Selim Dalkilic

Published by Yıldız Technical University Press, İstanbul, Turkey

INTRODUCTION

The flow pattern of fluid motion will vary depending upon the conduit and the environs which it presents. If the fluid is subjected to the multiphase fluid with the nature of immiscibility, its flow behaviour depends on the adjacent fluid also. Many researchers were involved in studying the immiscible characteristics of the fluids which undergone certain circumstances. Immiscible fluids are two or more fluids that are incapable of forming a homogeneous mixture or solution when combined. Because, immiscible properties are possessed by the strong intermolecular force of one fluid over another, different densities, viscosity, molecular structures and polarities. So, it is restricted to providing an adherence nature. These kinds of fluids are seen in our day-to-day life. In the biological system, the flow of blood in blood vessels, and food through the alimentary canal and in Industrial applications, emulsion formation, the extraction process, separation techniques, lubrications, fuel and cleaning and degreasing. The experimental work on the two-phase viscous flow in the case of oil pipelines was investigated by Michael Bentwich [1]. He performed this experiment in order to reduce the pumping costs. This research has concluded that the potentiality of the solution was made a valuable acceptance and this method produces the analogue to various problems in the fields of elasticity, heat and mass transfer, mechanics and the electric potential distribution. Following the validation of experimental work, Packham and Shail [2] were inspired to study the flow of two immiscible viscous fluids in the long horizontal pipe which is independent of time. He made a statement that the influence of the interface region between two fluids was very effective during the flow in a fully developed region because of the symmetricity of the conduit. On behalf of bio-rheological applications, Chaturani and Ponalagusamy [3] studied the behaviour of blood flow in the stenosed arteries by pondering blood vessels as a two-layer model. In the presence of a porous region, Srinivasan and Vafai [4] started the pioneer studies on the theoretical analysis of the two immiscible fluids. Furthermore, they made a statement about the physical importance of the porous material and flow effects in the presence of porous material. Following them, Chamkha [5] distinguished the difference between flow traits of electrically conducting two-phase immiscible fluids in the presence of porous and non-porous regions in the symmetric channel. In addition to that, the impact of electrically conducting fluids was more efficient in the porous region than in the non-porous region. Umavathi et al. [6] investigated the two-phase immiscible viscous fluids under the unsteady oscillatory motion along with heat transfer through a horizontal channel in the presence of an isothermal permeable wall. Meanwhile, the laminar condition on the fluid flow was very important to investigate in the case of two-phase immiscible fluids in order to utilize the bio-engineering fields like microchips, biochips, Lab-on-Chip etc..,. Based on this statement, Umavathi et al. [7] intervened in the motion of two immiscible viscous fluids in the long vertical wavy channel under the laminar condition. Prathap Kumar et al. [8] formulated the analytical solution of free convective two-layer immiscible micropolar and viscous fluids through the vertical channel. Ponalagusamy and Tamil Selvi [9] intervened in the stenosed arteries in the form of two-layered (Casson-Newtonian) blood flow along with variable slip wall conditions by assuming the axisymmetric cylindrical tube. Using a perturbation technique, Umavathi and Shekar [10] the mixed convective of fully developed laminar flow was interpreted by assuming different conductivity and viscosity in the two-layer viscous immiscible fluids. Along with the different aspects of immiscible fluids, it becomes necessary to analyse the immiscible combination of Newtonian and no-Newtonian. Such studies made a huge impact on industrial applications. Devakar and Ramgopal [11] performed an analytical study on immiscible fluids like Couple-stress fluid and Newtonian fluid through the circular cylinder in the presence of both porous and non-porous regions by assuming the condition axisymmetric nature. In the presence of particles or contamination, the fluids are assumed to be micropolar and the immiscible nature of micropolar-Newtonian in the porous region through the circular conduit in the axisymmetric condition has been analysed by Yadav and Verma [12]. Considering an optimal amount of density difference, the miscible nature of high-viscosity fluid with low-viscosity fluid was analysed by Akbari et al. [13]. Gemma Houston et al. [14] investigated the microfluidic devices that have dealt with miscible characteristics of the fluids and the experiments were also carried out in well-acceptable optimized value. The magnetohydrodynamics flow of variable viscosity in the two-phase model was analysed in the configuration of blood flow through the stenosed arteries analytically using the Frobenius method by Ponalagusamy [15].

Initially, several authors deal with Newtonian fluid under various circumstances. Newtonian fluid with two different viscosities possessing an immiscible nature was investigated by Rao et al. [16] under peristaltic motion. Vajravelu et al. [17] discussed the unsteady immiscible Newtonian fluid under a magnetic field between the permeable beds. The corrugated vertical channel was analysed using the perturbation technique by Umavathi et al. [18]. Using MHD flow in the isothermal wall, Dragiša D. Nikodijević et al. [19] interpreted the three immiscible fluids in a channel subjected to the horizontal position. In the periodically constricted tube with constant pressure, the immiscible Newtonian fluids were studied by Fraggedakis et al. [20]. Abd Elmaboud [21] analysed the impact of the magnetic field in a vertical semi-corrugated channel for two immiscible fluids. The combined effect of non-Newtonian and Newtonian fluids was considered an immiscible property and the interpretation was carried out in various circumstances. Devakar and Ramgopal [22] studied the immiscible flow of couple stress- Newtonian fluid in the

presence of porous and non-porous medium through a tube. The discussion of multiphase fluid immiscible models like micropolar-Newtonian fluid was interpreted under the assumption of unsteady motion and heat transfer by Devakar and Ankush Raje [23]. From the perspective of various liquid combination models subjected to immiscible nature, viscoelastic effects were studied by Seng Hoe Hue et al. [24]. Shan Fang et al. [25] made discussion in a pore doublet model, the immiscibility was interpreted by considering the effects of geometric structure also. The investigation on the unsteady flow of two immiscible electromagnetic effects in the porous medium by Sangeetha and Ponalagusamy [26].

Owing to this fact, the real-life application is probably based on non-Newtonian fluids. Non-Newtonian fluids contain variable viscosity, yield stress, non-linear shear rate components and other parameters. Depending on the fluid nature, a suitable non-Newtonian fluid will be taken to model. In both the biomedical and industrial fields, the fluids possessed non-Newtonian behaviour. Because the immiscible nature only occurs in the presence of highly complex molecular structures. Some of the non-Newtonian fluids are Power-law fluid, K-L model, Sutterby fluid, Casson fluid, Quemada model fluid, Jeffrey fluid, Thixotropic fluid, Hershey-Bulkley fluid, second-order fluid, Bingham fluid, etc.., were made simulation by various researchers using various techniques. Akbari et al., intervened in the flow of micropolar fluid on the linearly stretched porous sheet using a homotopy perturbation technique [27]. Applying Akbari-Ganji's Method on the complex two-phase nanofluids on the revolving system in the presence of a uniform magnetic field was investigated by Gholinia et al. [28]. Implanting the highly precision numerical method known as a variational iterative method, convective 2D micropolar fluid flow in the permeable channel was probed by Gholinia et al. [29]. On a theoretical basis, Dewangan et al., studied the superficial velocity and the temperature ratio of two-phase stratified fluid flow through the horizontal channel using the ANSYS fluent [30]. Özkan et al., experimentally computed the utilization of nanofluids on the conventional reinforced materials to analyse the mechanical efficiency of the wind turbine [31]. Employing the spectral collocation method, the computation analysis of the thermal conductance of the fluid properties has been carried out on the Casson nanofluid flow in the presence of variable magnetic field Akaje et al. [32]. Hattab et al. [33] interpreted the flow of convective magnetohydrodynamics of carbon nanotube and water as base fluid with the isothermal fins under the uniform magnetic field using a finite control volume method in the square enclosed conduit.

Among all other non-Newtonian models, the K-L model equation consists of three parameters which were experimentally verified by Luo and Kuang [34]. The model was constructed by analysing the shear-thinning behaviour of human blood. By using the weighted least square method, they formulated the constitutive equations with experimental data and this model satisfies with shear thinning characteristics of blood with high and low shear rates. Based on the human blood component, the variables present in this model are the yield stress and functions of blood components like hematocrit, the viscosity of plasma component and other additional chemical variables. The comparative analysis of the Casson fluid was made by Zhang and Kuang [35] experimentally by making certain modifications in the K-L model proving that it is far better than providing the pseudoplastic properties than the Casson fluid. Mostly, the K-L model has been dealing with blood flow behaviour. Somchai Sriyab [36] investigated the K-L blood flow in the stenosis and the narrow arteries region. In the presence of a non-symmetrical stenosed narrow artery, characteristics of the blood (K-L model) flow were analysed by Rekha Bali and Nivedita Gupta [37]. Ponalagusamy and Ramakrishna Machi [38-40], dealt with the two-layered (K-L- Newtonian) blood flow of mild stenosed arteries in six various types, in the presence of porous walls with stenosed arteries and pulsatile flow in the tapered stenosis as single-layer K-L model. Using Aris's method of moments, Shalini Singh and Murthy [41] have investigated the unsteady behaviour of solute dispersion in the pulsatile K-L fluid motion in the rigid circular conduit. In this examination, they computed the higher order moments like the 3rd and 4th central moments for the mean concentration and found that the dispersion of the solute provides precise information for the higher order moments. By considering blood as a K-L model, the dispersion of soluble matter in blood flow has been analysed by Ponalagusamy et al. [42]. In these works, the impact of the electric field on the flow is not investigated. One can derive other types of fluids by making some components in appropriate measured values which will be discussed later.

As so far, in the prior prescribed discussion, the effect of an electrokinetic factor was least discussed. While dealing with the electrically conducting fluid, it is possible to make a single-phase or multi-phase fluid undergone for the external electric field. Electrokinetic effects have a wide range of applications. Mechanism-based on the electroosmotic phenomena is when the wall of the tube is charged with positive (or negative), the fluid present in the tube can move counter ions near the wall. It tends to form a strong bond near the wall. Due to the external electric field, it possesses a strong electric field near the wall and tends to form the second layer. These layers are called the electric double layer.

Based on this electrostatic phenomenon, many authors interpret based on various kinds of fluid. In the existence of an external electric field, the motion of two immiscible fluids in the microchannel was examined by Gao et al. [43]. Zhao and Yang [44] discussed the behaviour of electrokinetic phenomena applied to the Newtonian fluid in detail. Afonso et al. [45] investigated analytically the two-phase electro-osmotic flow of stratified fluids based on the behaviour of viscoelastic nature. In the formation of

electroosmotic flow with multilayer fluid in the existence of a peristaltic effect, many authors discussed. In the existence of peristaltic motion in the wall, two-layered: Power Law and Newtonian models were discussed by Goswami et al. [46]. Considering the two immiscible fluid flows consisting of the electrically conducting fluid and non-conducting fluids subjected to Newtonian fluid was discussed by Harshad Gaikwad et al. [47] presented their work analytically. Mithilesh et al. [48] proposed the bio-rheological factors of micropolar fluids through the microfluidic channels with peristaltic wave walls under the electro-osmotic flow. Based on the peristaltic motion, the Ellis-Newtonian model was investigated by Ali et al. [49] and Hussain and Ali [50] analysed the Multilayer Power-law. Ponalgusamy and Sangeetha [51] interpreted the flow characteristic of the two-phase (Thixotropic- Newtonian) model in the presence of electroosmotic force. Furthermore, the influence of the electro-osmotic effect on several characteristic assumptions was carried out by many authors. The pulsatile nature of nanofluid in the microchannel was analysed by Mukherjee et al. [52]. Tanoy Kahali et al. [53], interpreted the trajectory of a compound drop in a microfluidic channel and numerical investigations were performed by Mid Ismaveel et al [54], by assuming the Electrodiffusio-osmotic transport in nanochannels under various parameters. Followed by fellow researchers, the effective motion of electrically conducting-non-conducting immiscible fluids has been computed analytically using periodic motion on electric under the external impact of the magnetic field was formulated by Ponalagusamy and Sangeetha [55]. Sangeetha et al. [56], computed the electric field impact on the time-dependent peristaltic motion of two-phase immiscible fluids in the elastic tube using the perturbation technique under the magnetic field through the porous medium. In this case, they analyse the influence of the electroosmotic effect at the interface region. The impact of electroosmotic force in electrically conducting fluids is worth noticing. In this case, the electroosmotic effect on the peristaltic motion of immiscible flow in the circular conduit along with the variable viscosity coefficient has been studied analytically by Sangeetha et al. [57].

In the aforementioned studies, the interpretation of the immiscible fluids becomes very complex when dealing with the combined effects of non-Newtonian and Newtonian fluids, particularly the non-Newtonian fluids since it consists of highly complex structures in nature. On behalf of dealing with other non-Newtonian fluids which possess a viscoelastic nature, the K-L model proposed by Kuang and Luo was purely done by the experimental process based on the human and canine blood and its properties formulating the equations using the empirical formula using the values of apparent viscosity, shear rate and yield stress. So far, the studies have not described the limitations while dealing with the K-L parameters. In our research, the formulation of the limiting case was carried on with the suitable mathematical condition. Moreover, the impact of external body forces like an electrokinetic body force made an efficient flow in the prescribed conduit which is also considered in this work. Inspired by these quantities, the model was constructed in a possible way which suggests dealing with the industrial-based application under different environments. Therefore, the analysis is mathematically modelled by two-layered immiscible flow in the existence of the external electric field. The mid region represents K-L fluid and the outer region is Newtonian fluid. The mathematical formulation of velocity profiles, fluid flow rate, the plug core radius and the wall shear stress are expressed analytically with properly prescribed boundary conditions. Our present investigation became the generalized model of certain non-Newtonian fluids like Casson fluid, Bingham fluid and Newtonian fluid.

MATHEMATICAL FORMULATION

Geometrical Description

Consider the steady-state, axisymmetric, incompressible, laminar and two-phase motion of immiscible fluids subjected to the electrically conducting properties through the cylindrical coordinate system (r_1^*, θ_1^*, z_1^*), where r_1^* represents the direction towards the radial distance, θ_1^* indicates the direction over the circumferential rotation and z_1^* denotes the direction of the axial distance. Meanwhile, the flow towards θ_1^* Direction dissipated because of the axisymmetric nature of the model. Based on the above assumptions, the motion in the present model projects the unidirectional way in the axial distance. The suggested model contains two sections: the mid-area named as K-L fluid model and the outer sector named Newtonian fluid. In Figure 1, the configured shape of the presently studied two-phase model is exhibited in a well-manner form.

Charge Distribution in the Pipe

In order to analyse the charge distribution, certain assumptions need to be taken into account. The surface of the tube should be homogenous. In heterogeneous material used, the charge distribution over a concern region will vary and it might cause variation in flow pattern. Owing to the phenomena of electrostatic theory, the formulation to construct the potential charge distribution which leads to the disposition of an Electric Double Layer (EDL) at the surface of the wall which obeys the linearized form of Poisson-Boltzmann equation,

$$\varepsilon^* \nabla^2 \psi^* = -\rho_e^* \tag{1}$$

where ψ^* denoted the potential distribution of electric force, ε^* represents the permittivity of the medium and ρ_e^* indicates the net charge density which formulated as $\rho_e^* = ez^{\pm}(n^+ - n^-)$. Here, the components present in the net charge density were composed of the electric charges (e), the valence of the respective charged ions ($z^{\pm}$) and the

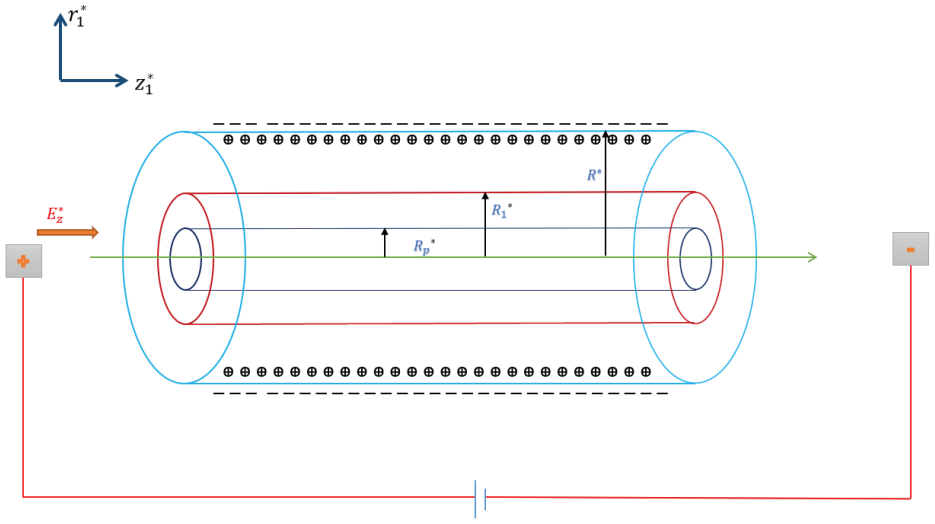

Figure 1. A visual depiction of the prescribed mathematical model in schematic form. In the current study, the wall of the tube assumed as negatively charged and the fluid area has a net positive charge which stabilises the surface charge.

number of the density of ions and counterions ($n^{\pm}$). Since, the fluid flow acquaintance with the additional body force term namely electrokinetic force because of the external electric field E_z^* [55-57].

$$F_{EK}^* = -\rho_e^* E_z^* \tag{2}$$

Fluid Flow for Velocity Distribution

The corresponding continuity and the momentum equations present in both the regions are displayed as follows:

i. For core region (K-L fluid): $0 \le r_1^* \le R_1^*$

$$\frac{\partial w_{11}^*}{\partial z_1^*} = 0 \tag{3}$$

$$-\frac{\partial p_0^*}{\partial z_1^*} - \frac{1}{r_1^*}\frac{\partial}{\partial r_1^*}\left(r_1^*\left|\tau_{r_1^* z_{11}^*}^*\right|\right) + F_{EK}^* = 0 \tag{4}$$

ii. For peripheral region: $R_1^* \le r_1^* \le R^*$

$$\frac{\partial w_{12}^*}{\partial z_1^*} = 0 \tag{5}$$

$$-\frac{\partial p_0^*}{\partial z_1^*} + \frac{1}{r_1^*}\frac{\partial}{\partial r_1^*}\left(r_1^*\tau_{r_1^* z_{12}^*}^*\right) + F_{EK}^* = 0 \tag{6}$$

where w_{11}^*, w_{12}^* epresents the velocity distribution occupies the areas of the core and the peripheral layers in the axial direction, r_1^* is the length of the radial direction and $-\frac{\partial p_0^*}{\partial z_1^*}$ indicated the pressure gradient. "*" implies the dimensional quantities.

The constitutive equation for the corresponding fluids is given as

$$\tau_{r_1^* z_{11}^*}^* = \tau_0^* + \eta_2^*\gamma^* + \eta_1^*\sqrt{\gamma^*}\,; \quad \tau_{r_1^* z_{11}^*}^* > \tau_0^* \tag{7}$$

$$\frac{\partial w_{11}^*}{\partial z_1^*} = 0\,; \quad \tau_{r_1^* z_{11}^*}^* \le \tau_0^* \tag{8}$$

$$\tau_{r_1^* z_{12}^*}^* = \mu_n^*\frac{\partial w_{12}^*}{\partial r_1^*}\,; \tag{9}$$

where the stress components act in the $r_1^* z_1^*$ plane, τ_0^*, η_1^*, η_2^*, $\gamma^*$and μ_n^* are yield stress and functions of the blood components like hematocrit, the viscosity of plasma components, other additional chemical variables, shear rate and viscosity in the Newtonian region respectively.

The relative boundary condition in the dimensional form is

i) at $r_1^* = 0;\ \tau_{r_1^* z_{11}^*}^*$ is finite (10)

ii) at $r_1^* = R_p^*;\ \frac{\partial w_{11}^*}{\partial z_1^*} = 0$ (11)

iii) at $r_1^* = R_1^*;\ w_{11}^* = w_{12}^*;\ \tau_{r_1^* z_{11}^*}^* = \tau_{r_1^* z_{12}^*}^*$ (12)

iv) at $r_1^* = R^*; w_{12}^* = 0$ (13)

where R_p^*, R_1^* and $R^*$are plug core radius, interfacial thickness and height of the tube from the axial direction to the outer wall. Solving the momentum equations using the respective boundary conditions, the following dimensional

quantities have been implemented to make the non-dimensional form,

$$r_1 = \frac{r_1^*}{R^*};\ z_1 = \frac{z_1^*}{R^*};\ R_1 = \frac{R_1^*}{R^*};\ w_{11} = \frac{w_{11}^*}{U^*};$$
$$w_{12} = \frac{w_{12}^*}{U^*};\ p_0 = \frac{R^*}{U^*\mu_n^*}p_0^*;\ \tau_{r_1z_{11}} = \frac{R^*}{U^*\mu_n^*}\tau_{r_1^*z_{11}^*};$$
$$\tau_0 = \frac{R^*}{U^*\mu_n^*}\tau_0^*;\ F_{EK} = \frac{R^{*^2}}{\varepsilon^*\zeta^*\mu_n^*}F_{EK}^*;\theta_1 = \frac{\eta_1^*}{\mu_n^*}\sqrt{\frac{R^*}{U^*}};\ \theta_2 = \frac{\eta_2^*}{\mu_n^*}$$

where $U^*$is reference velocity.

The dimensionless governing equations are as follows,

i. For core region: $0 \le r_1 \le R_1$

$$\frac{\partial w_{11}}{\partial z_1} = 0 \tag{14}$$

$$-\frac{\partial p_0}{\partial z_1} - \frac{1}{r_1}\frac{\partial}{\partial r_1}\left(r_1\left|\tau_{r_1z_{11}}\right|\right) + U_e\rho_e = 0 \tag{15}$$

ii. For peripheral region: $R_1 \le r_1 \le 1$

$$\frac{\partial w_{12}}{\partial z_1} = 0 \tag{16}$$

$$-\frac{\partial p_0}{\partial z_1} + \frac{1}{r_1}\frac{\partial}{\partial r_1}\left(r_1\frac{\partial w_{12}}{\partial r_1}\right) + U_e\rho_e = 0 \tag{17}$$

where $U_e = -\frac{\varepsilon^*\zeta^*E_z^*}{\mu_n^*}$ is an electrokinetic slip velocity [39,42-44,50].

The constitutive equation (non-dimensional form) is given as

$$\tau_{r_1z_1} = \tau_0 + \theta_1\sqrt{-\frac{\partial w_{11}}{\partial r_1} - \theta_2\frac{\partial w_{11}}{\partial r_1}};\quad \tau_{r_1z_1} > \tau_0 \tag{18}$$

$$\frac{\partial w_{11}}{\partial r_1} = 0;\qquad \tau_{r_1z_1} \le \tau_0 \tag{19}$$

where θ_1, θ_2 and τ_0 are the K-L parameters and yield stress. The respective boundary conditions are

i) at $r_1 = 0;\ \tau_{r_1z_{11}}$ is finite (20)

ii) at $r_1 = R_p;\ \frac{\partial w_{11}}{\partial r_1} = 0$ (21)

iii) at $r_1 = R_1;\ w_{11} = w_{11};\ \tau_{r_1z_{11}} = \tau_{r_1z_{12}}$ (22)

iv) at $r_1 = 1;\ w_{12} = 0$ (23)

To solve the aforementioned non-linear momentum equations, two kinds of techniques have been invoked i.e. either the solution of the equation can be obtained by momentum equation in addition to the electro-kinetic body force term or to transfer its participation in the form of suitable boundary conditions at the outer wall as electro-kinetic slip parameter [46,49-51,57]. In this study, we opt for the second type by shifting the electro-kinetic body force term to the no-slip boundary condition at the conduit wall, and then boundary condition (23) becomes

$$\text{at } r_1 = 1;\ w_{12} = U_e \tag{24}$$

After transferring the slip parameter, the momentum equations become

$$-\frac{\partial p_0}{\partial z_1} - \frac{1}{r_1}\frac{\partial}{\partial r_1}\left(r_1\left|\tau_{r_1z_{11}}\right|\right) = 0 \tag{25}$$

$$-\frac{\partial p_0}{\partial z_1} + \frac{1}{r_1}\frac{\partial}{\partial r_1}\left(r_1\frac{\partial w_{12}}{\partial r_1}\right) = 0 \tag{26}$$

The Analytical Expression for the Solution

Solving the momentum equations (25) and (26), applying the boundary conditions (20)-(22) and (24), the mathematical expression of the velocity distribution in the two sectors is obtained as

In $R_p \le r_1 \le R_1$.

$$w_{11} = \frac{P}{4\theta_2}(\theta_2 + R_1^2(1-\theta_2) - r_1^2) + \frac{1}{2\theta_2^2}(2\tau_0\theta_2 - \theta_1^2)(r_1 - R_1) + \frac{\theta_1}{6P\theta_2^3}\left((\theta_1^2 + 2\theta_2 Pr_1 - 4\theta_2\tau_0)^{3/2} - (\theta_1^2 + 2\theta_2 PR_1 - 4\theta_2\tau_0)^{3/2}\right) + U_e \tag{27}$$

In $R_1 \le r_1 \le 1$:

$$w_{12} = \frac{P}{4}(1 - r_1^2) + U_e \tag{28}$$

The rate at which fluid is moving in the plug-core region is

In $0 \le r_1 \le R_p$:

$$w_{11} = \frac{P}{4\theta_2}\left(\theta_2 + R_1^2(1-\theta_2) - R_p^2\right) + \frac{1}{2\theta_2^2}(2\tau_0\theta_2 - \theta_1^2)(R_p - R_1) + \frac{\theta_1}{6P\theta_2^3}\left((\theta_1^2 + 2\theta_2 PR_p - 4\theta_2\tau_0)^{3/2} - (\theta_1^2 + 2\theta_2 PR_1 - 4\theta_2\tau_0)^{3/2}\right) + U_e \tag{29}$$

where $P\left(= -\frac{\partial p_0}{\partial z_1}\right)$ is pressure gradient and R_p is the radius of the plug-core region formulated as $R_p = \frac{2\tau_0}{P}$. The flow flux of a given region, Q (in non-dimensional form) is

$$Q = 2\int_0^{R_p} r_1 w_{pc} dr + 2\int_{R_p}^{R_1} r_1 w_{11} dr + 2\int_{R_1}^{1} r_1 w_{12} dr$$

$$\begin{aligned} Q = &-\frac{PR_p^4}{8\theta_2} - \frac{2\tau_0\theta_2 - \theta_1^2}{3\theta_2^2} R_1 R_p^2 + \frac{P}{8\theta_2}(R_1^4(1-\theta_2)+\theta_2) + \frac{2\tau_0\theta_2 - \theta_1^2}{6\theta_2^2} R_1^3 \\ &- \frac{\theta_1^6}{105P^3\theta_2^5}(14\tau_0\theta_2 P - \theta_1^2) + \left(A + 2\theta_2 P R_p\right)^{\frac{3}{2}}\left(R_p^2 - R_1^2\right) \\ &+ \frac{2R_1}{5\theta_2 P}(A + 2\theta_2 P R_1)^{\frac{5}{2}} - \frac{2R_p}{5\theta_2 P}(A + 2\theta_2 P R_p)^{\frac{5}{2}} \\ &+ \frac{2}{35\theta_2^2 P^2}(A + 2\theta_2 P R_p)^{\frac{7}{2}} - \frac{2}{35\theta_2^2 P^2}(A + 2\theta_2 P R_1)^{\frac{7}{2}} + U_e \end{aligned} \quad (30)$$

where $A = \theta_1^2 - 4\theta_2\tau_0$.

By assuming the flow flux (Q) value, the corresponding pressure gradient (P) values have been calculated with suitable values of the other parameters using MATLAB programming. By using the equations (31) and (28), one can obtain the expression for τ_w,

$$\tau_w = \left(-\frac{dw_{12}}{dr_1}\right)_{r_1=1} \quad (31)$$

VALIDATION RESULTS

The flow of the two-phase immiscible fluids through the circular tube which was mentioned above has a tendency to perform like a generalized form of other fluid models, viz Newtonian-Newtonian, Bingham Plastic-Newtonian and Casson-Newtonian models with certain restrictions of the provided parameters.

Newtonian-Newtonian

The flow flux of the Newtonian-Newtonian model can be obtained by vanishing the yield stress (τ_0) and K-L parameter (θ_1) and the constitutive equation of the core region (K-L Fluid) behaves like a Newtonian fluid and its flow rate given as follows.

$$Q = \frac{P}{8\theta_2}(R_1^4(1-\theta_2)+\theta_2) + U_e \quad (32)$$

Bingham-Newtonian

The flow flux of the Bingham-Newtonian model can be obtained by vanishing the K-L parameter (θ_1) and the constitutive equation of the core region (K-L Fluid) behaves like a Bingham fluid and its flow rate given as follows.

$$Q = \frac{P}{8\theta_2}\left(R_1^4 - R_p^4\right) - \frac{\tau_0}{3\theta_2}\left(R_1^3 - R_p^3\right) + \frac{P}{8}(1 - R_1^4) + U_e \quad (33)$$

Casson-Newtonian

The flow flux of the Casson-Newtonian model can be obtained by formulating the K-L parameter (θ_1) as $2\sqrt{\tau_0\theta_2}$ (i.e.) $\theta_1 = 2\sqrt{\tau_0\theta_2}$ and the constitutive equation of the core region (K-L Fluid) behaves like a Casson fluid and its flow rate is given as follows

$$\begin{aligned} Q = &-\frac{PR_p^4}{8\theta_2} + \frac{\tau_0}{3\theta_2}\left(R_1^3 + R_p^3\right) + \frac{P}{8}\left(1 - R_1^4 + \frac{R_1^4}{\theta_2}\right) \\ &+ \frac{\sqrt{8\tau_0 P}}{3\theta_2} R_p^{7/2} - \frac{7\sqrt{8\tau_0 P}}{21\theta_2} R_p^{7/2} - \frac{6\sqrt{8\tau_0 P}}{42\theta_2} R_1^{7/2} + U_e \end{aligned} \quad (34)$$

Graphical Validation

The graphical outcome of the present model was compared with the existing analytical model in three different cases:

(i) Velocity profile of different values of hematocrit with no electric osmotic flow [38].
(ii) Two-phase flow of K-L-Newtonian model along with the absence of electric field [38].
(iii) The one-layer flow of the K-L-Newtonian model with no electrokinetic effect [40].

Ramakrishna Manchi and Ponalagusamy [38] derived the analytical solution for steady-state two-phase K-L-Newtonian fluid in the human stenotic artery region with no-slip boundary condition. Ramakrishna Manchi and Ponalagusamy [40] discussed the pulsatile flow of K-L fluid through the stenotic region as a one-layer model analytically. Validation of the velocity profiles for the current study was evaluated from three different perspectives. First, the non-stenotic region of the hematocrit velocity in the absence of an electric field by Ramakrishna Manchi and Ponalagusamy [38] is displayed in Figure 2. Second, the two-phase velocity profiles of the K-L-Newtonian model (with no electroosmotic effect) are presented in Figure 3. Third, Figure 4 shows the validation of the one-layer model which was studied by Ramakrishna Manchi and Ponalagusamy [40] in the non-stenotic region with zero electroosmotic force. Moreover, the velocity profile values of our present work for the one-layer model were in good agreement with the existing work which is shown in Table 1. It is noticed that our results were well matched with the analysis carried out earlier by Ramakrishna Manchi and Ponalagusamy [40].

Observation and Outcomes

In the current analysis, the flow of immiscible fluids is constructed in the two-layered model with K-L fluid occupying the inner region and the outer region confined by the Newtonian fluid. The investigation was made on the flow characteristics of two electrically conducting fluids actuated by the combined effects of electro-osmotic and pressure forces under the influence of the Electric double layer (EDL) effect formed at the wall. The flow behaviour of the fluids in the form of velocity profile, flow flux, plug core radius and skin friction components have been investigated. The numerical computation of the velocity, flux, wall shear stress and plug core radius equations can be wisely calculated using the Matlab software package which will be useful for the graphical representation of the flow pattern. Yield stress, peripheral layer thickness, and electric field will have a preponderance of impacts across the tube, and

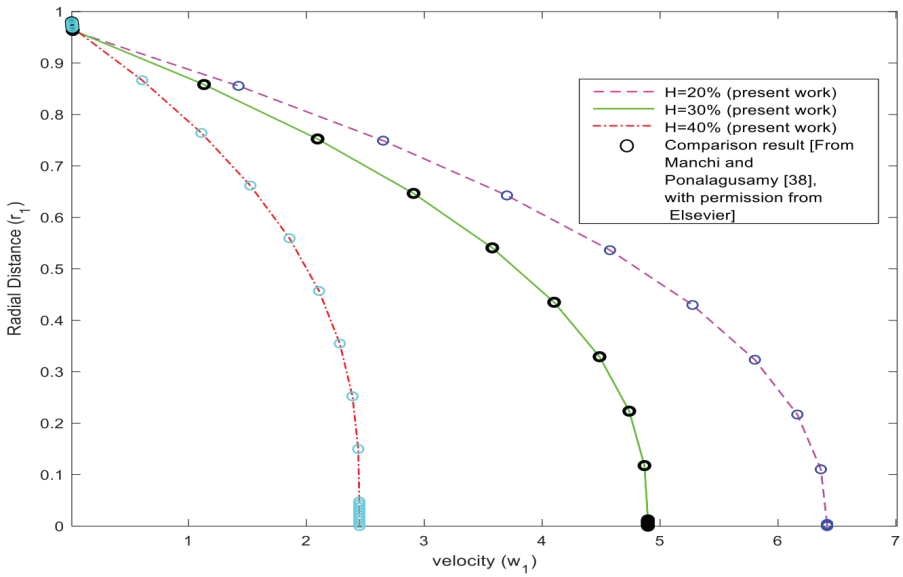

Figure 2. Velocity profiles for different values of hematocrit of the current model compared with the velocity profiles of the non-stenotic region of the two-layer model. [From Manchi and Ponalagusamy [38], with permission from Elsevier].

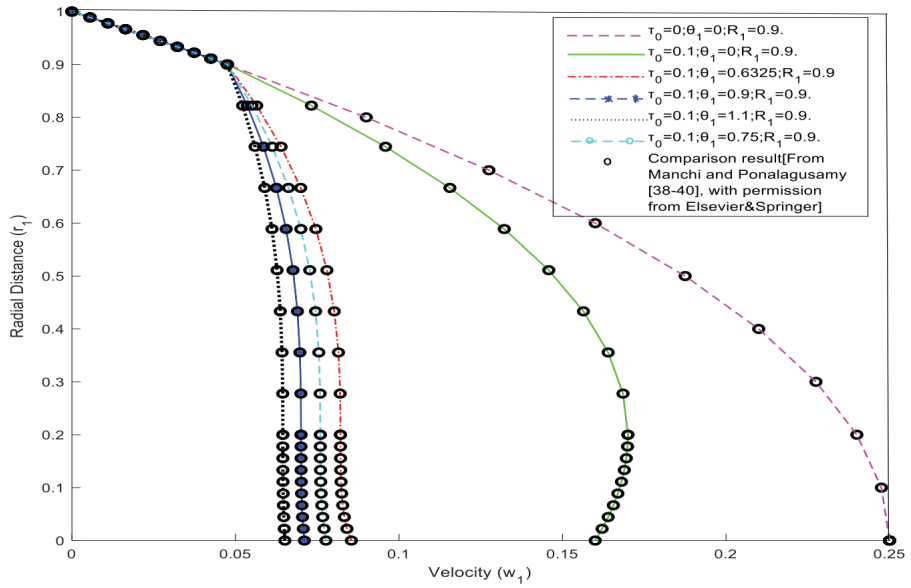

Figure. 3. Velocity profiles of the current model compared with the velocity profiles of the non-stenotic region of the two-layer model. [From Manchi and Ponalagusamy [38], with permission from Elsevier].

we bring out the eminence effects of the flow dynamics, which depend on K-L parameters, and the discussion will be carried out in upcoming figures along with the values prescribed in Table 2.

The components present in the K-L constitutive equation are constructed using the empirical formula of experimental values obtained from the human and canine blood samples like the Quemada model, Bi-Exponent model, Casson model and Power-law model [34]. The apparent viscosity, shear rate and yield stress of the hemorheology provide the better approximate result in K-L Blood Constitutive equations (BCEs) compared to the Casson model. Here, the parameters present in the K-L model, θ_1 represents the relative viscosity that may be related to the aggregative level of Red Blood Cells and θ_2 denotes the viscosity index that may be related to the aggregation of Red Blood Cells. Since there are many BCEs but that cannot be directly related to the aggregation and deformability of RBC it is necessary to

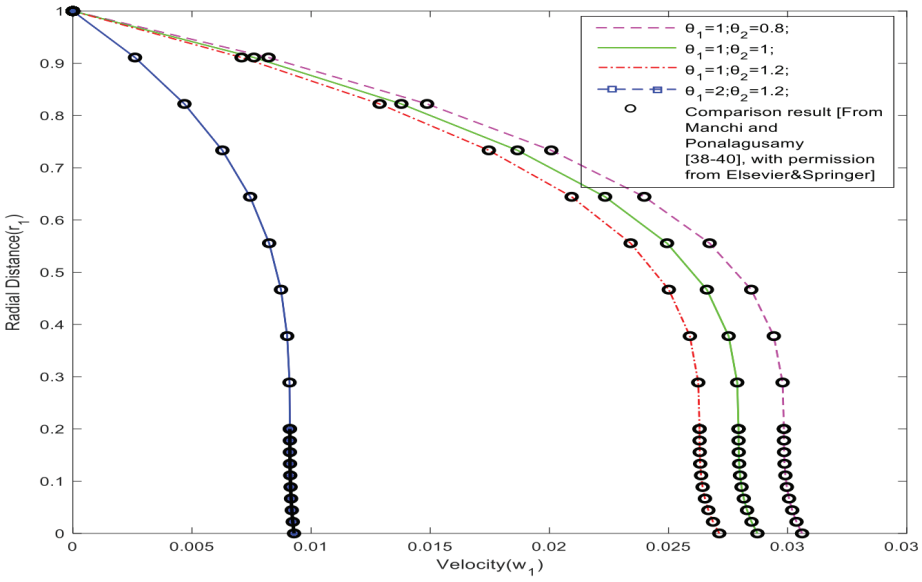

Figure 4. Velocity profiles of the current model compared with the velocity profiles of a non-stenotic region of a one-layer model.[From Manchi and Ponalagusamy [38-40], with permission from Elsevier & Springer].

Table 1. Velocity profiles of the current model compared with the velocity profiles of the non-stenotic region of the one-layer model. [From Manchi and Ponalagusamy [40], with permission from Springer]

$\theta_1 = 2; \theta_2 = 1.2$		$\theta_1 = 1; \theta_2 = 1.2$		$\theta_1 = 1; \theta_2 = 1$		$\theta_1 = 1; \theta_2 = 0.8$	
Manchi & Ponalagusamy [40]	**Present work**	**Manchi & Ponalagusamy [40]**	**Present work**	**Manchi & Ponalagusamy [40]**	**Present work**	**Manchi & Ponalagusamy [40]**	**Present work**
0	0	0	0	0	0	0	0
0.0051	0.0051253	0.0141	0.014130	0.0151	0.0151255	0.0163	0.01630061
0.0079	0.0078824	0.0223	0.0222899	0.0238	0.02376323	0.0255	0.02548836
0.0089	0.0088688	0.0257	0.025732	0.0274	0.0273547	0.0292	0.02292448
0.0091	0.0091084	0.0263	0.0263022	0.0279	0.02793766	0.0298	0.02984228
0.0091	0.00911110	0.0263	0.02631317	0.0279	0.02794848	0.0299	0.02985302
0.0091	0.0091297	0.0264	0.0263941	0.028	0.0280279	0.0299	0.02993105
0.0092	0.0091812	0.0266	0.0266301	0.0283	0.02825633	0.0302	0.03015238
0.0093	0.0092831	0.0271	0.0271265	0.0287	0.02873066	0.0306	0.03060477

Table 2. The magnitude of dimensionless parameters for the suggested model are displayed as follows

Parameters	**Range**	**References**
Electric field, U_e	0-1	Goswami et al. [46], Ali et al. [49], Hussain and Ali [50], Ponalagusamy and Sangeetha [51, 57].
Yield stress, τ_0	0-0.1	Ponalagusamy and Machi [38-40], Ponalagusamy and Sangeetha [51, 57].
K-L parameter, θ_1	0-1	Ponalagusamy and Machi [38-40].
K-L parameter, θ_2	0.01-1.5	Ponalagusamy and Machi [38-40].
Interface thickness, R_1	0.7-0.9	Ponalagusamy and Sangeetha [51].

find out a BCEs which can be related to RBC aggregation and deformability. Based on the human and canine blood samples, the root-mean-square differences between BCEs and the measured results are calculated. Among the BCEs, K-L equations provide more satisfactory results because of lesser RMS values [34],[35]. Inspired by this rheological model, these studies may provide an improvement on the research work-based industrial applications under the external electric field [41].

At this juncture, it is pertinent to observe from equation (27) that when $\theta_2 = 0$, the velocity of the core fluid becomes infinity which fails to represent the real flow phenomenon. Hence, the non-zero value of θ_2 should be considered for investigating its effect on the flow characteristics. The pressure force plays a significant role in dealing with the fluid motion. The pressure force was most prominently influenced by the yield stress (τ_0) and K-L parameters θ_1 and θ_2. It is computationally noticed that using equation (30) and for a given value of flow rate(Q), we cannot independently assign a value to τ_0, θ_1 and θ_2 while computing the numerical value of pressure gradient (P), otherwise, it is impossible to obtain acceptance value (real and positive) of the pressure gradient (P). It is observed that for a given value of the yield stress (τ_0), the acceptable pressure gradient values were obtained when $\theta_1 \leq \theta_2$, otherwise the existence of real roots vanished. This is mathematically attributed to the fact that the resultant polynomial equation in the form of a pressure gradient (P) obtained from equation (30) is of the fourth-degree equation if $\left|\frac{2\theta_2 PR_1}{\theta_1^2 - 4\theta_2\tau_0}\right| \leq 1$.

By considering the condition $\theta_1 > \theta_2$, the discriminant value of the fourth-degree polynomial equation was positive for the appropriate numerical values, and the corresponding roots obtained for this value are non-real roots, which were well matched with the discriminant condition. Without considering the constraint mentioned earlier, we computationally observed that when $\theta_1 > \theta_2$, the realistic value of pressure gradient for the prescribed model is impossible to obtain.

The axial velocity profiles in the radial direction are computed over the concerned parameters. Due to symmetricity, the investigation was carried out on the half region and the velocity profiles of both one-layered and two-layered models were scrutinized. The graphical representation of the velocity profiles was analysed under the various parameters shown in Figure 5- 8. In Figures 5 and 6, under the influence of the electric field, K-L parameter (θ_1) and yield stress an investigation of the velocity profile of two-layered and one-layered models was performed. In Figure 5, we analysed the four types of two-fluid models, such as Newtonian-Newtonian, Bingham-Newtonian, Casson-Newtonian (θ_2=1; $\theta_1 = 2\sqrt{\theta_2\tau_0}$) and K-L-Newtonian. The Casson -Newtonian fluid model can also be derived from any assigned value of the K-L parameter (θ_2). Compared to all the two-fluid models, Newtonian fluids are much faster than other fluids. When the yield stress increases it reduces the flow nature of the fluid. This fact is easily verified in the given figure. Moreover, the K-L parameter (θ_2) also possessed a greater influence on the flow nature. Witnessed, it has proven that the flow decreases, whenever

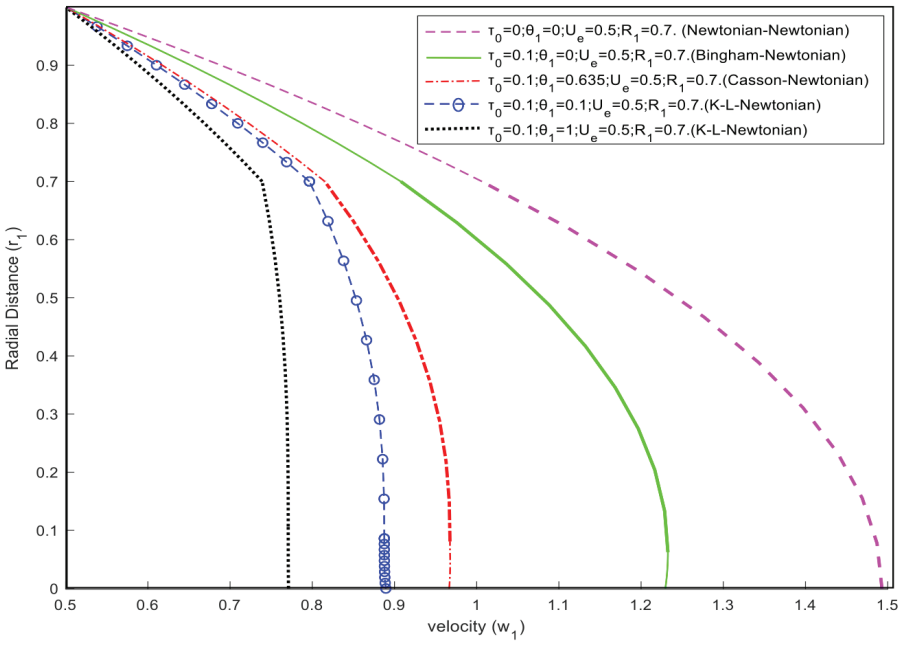

Figure 5. Velocity distribution along with radial direction for distinct values of yield stress (τ_0) and K-L parameter (θ_1). [two-layered model with θ_2=1; $\theta_1 \leq \theta_2$].

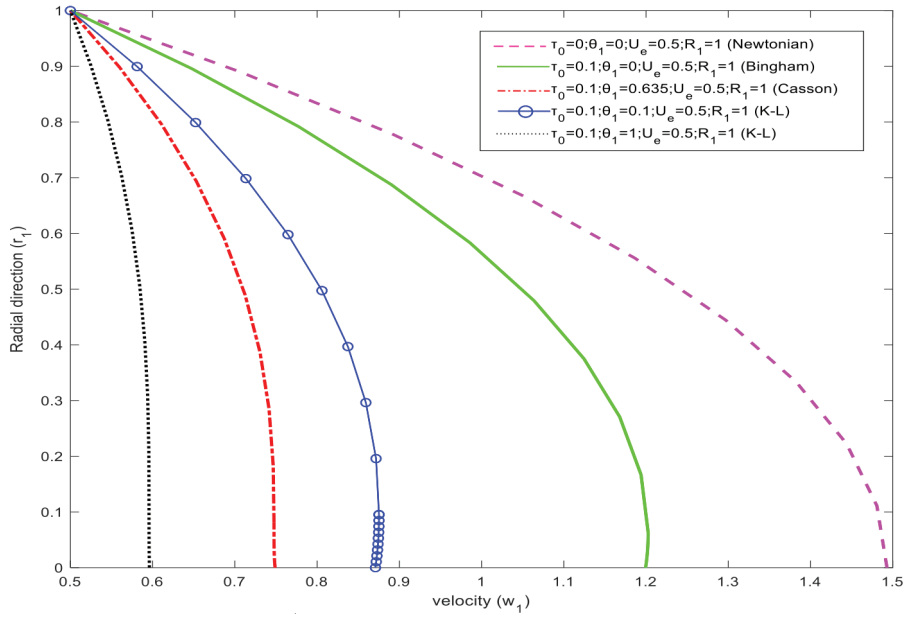

Figure 6. Velocity distribution along with radial direction for distinct values of yield stress (τ_0) and K-L parameter (θ_1). [one-layered model with θ_2=1; $\theta_1 \leq \theta_2$].

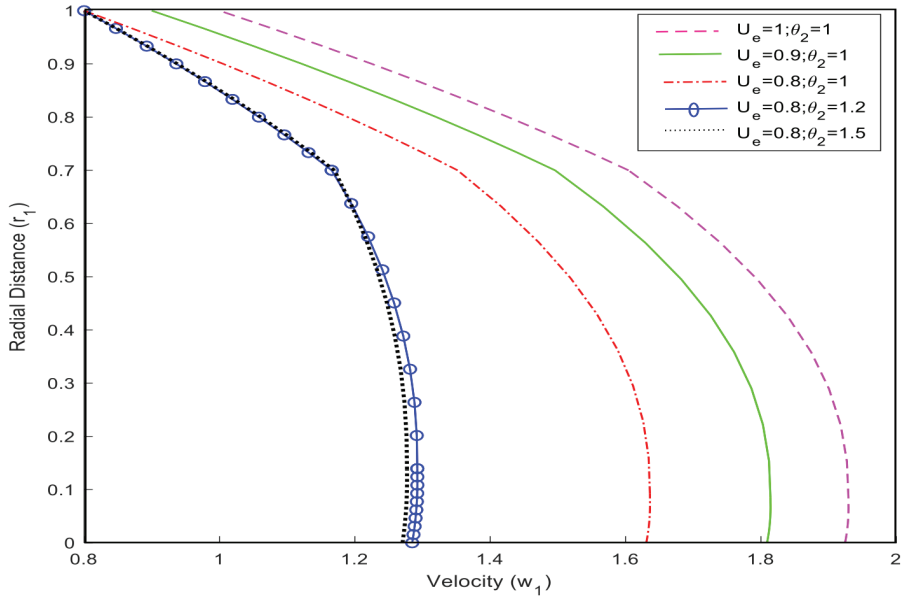

Figure 7. Velocity distribution along with radial direction for distinct values of K-L parameter (θ_2) and electric field (U_e).

θ_2 increases. Furthermore, θ_1 is the coefficient of the shear thinning component and it invokes the behaviour of the core fluid model. The higher the value of θ_1, the shear rate of pseudo-plasticity increases and hence velocity decreases. Moreover, it analysed that the two-layered Newtonian-Newtonian model is approximately higher than the Casson-Newtonian (6.74%), Bingham-Newtonian (17.92%) and K-L-Newtonian (22.77%) in velocity profiles along with the data points in Table 3.

In Figure 6, the distribution of velocity along the radial distance with the one-layer model is displayed. If the intermediate layer thickness (R_1) is enlarged or approaches the outer layer of the wall (R), then the fluid flow model is probably considered to be a one-layered model. The discussion made in Figure 6, is based on the yield stress (τ_0), K-L

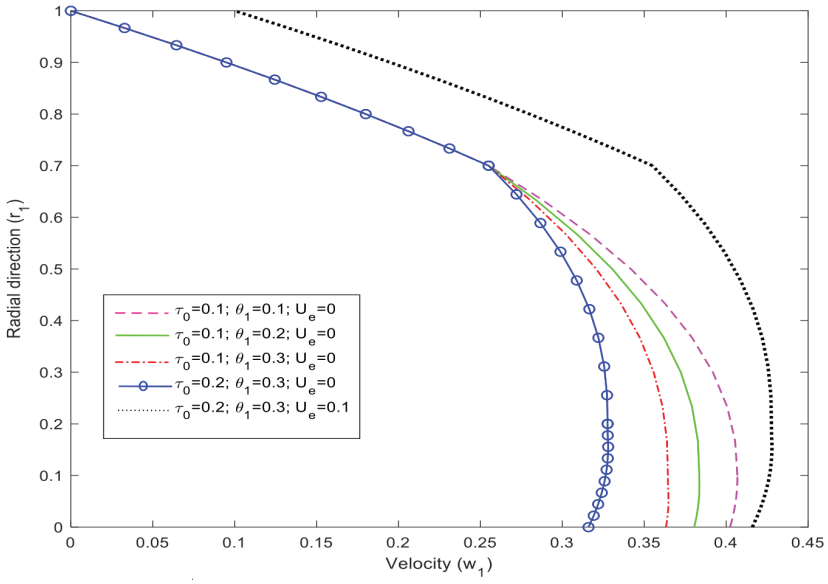

Figure 8. Velocity distribution along with radial direction for distinct values of yield stress (τ_0), K-L parameter (θ_1) and Electric field (U_e).

Table 3. Values for the velocity distribution along with radial direction for distinct values of yield stress (τ_0) and K-L parameter (θ_1) provided in Figure 5. [two-layered model with θ_2=1; $\theta_1 \leq \theta_2$]

Newtonian-Newtonian		Bingham-Newtonian		Casson-Newtonian		K-L-Newtonian (θ_1=1)		K-L-Newtonian (θ_1=0.1)	
y-axis	x-axis	y-axis	x-axis	y-axis	x-axis	y-axis	x-axis	y-axis	x-axis
1	0.5	1	0.5	1	0.5	1	0.5	1	0.5
0.96	0.5651	0.96	0.55	0.96	0.5405	0.96	0.53	0.96	0.5381
0.93	0.628	0.93	0.603	0.93	0.5797	0.93	0.56	0.93	0.5749
0.9	0.688	0.9	0.651	0.9	0.6175	0.9	0.58	0.9	0.6105
0.86	0.747	0.86	0.699	0.86	0.6539	0.86	0.616	0.86	0.6447
0.83	0.803	0.83	0.744	0.83	0.6889	0.83	0.6432	0.83	0.677
0.8	0.857	0.8	0.7878	0.8	0.7226	0.8	0.6688	0.8	0.7093
0.76	0.909	0.76	0.8296	0.76	0.7548	0.76	0.6932	0.76	0.7397
0.73	0.959	0.73	0.8695	0.73	0.7857	0.73	0.7162	0.73	0.7688
0.7	1.0064	0.7	0.9077	0.7	0.8153	0.7	0.7391	0.7	0.7966
0.62	1.1085	0.62	0.9759	0.631	0.8503	0.63	0.7476	0.63	0.8191
0.54	1.198	0.55	1.0361	0.56	0.8805	0.56	0.7546	0.563	0.8381
0.46	1.2767	0.48	1.088	0.49	0.906	0.502	0.7601	0.495	0.8537
0.38	1.34	0.41	1.1324	0.42	0.9268	0.436	0.7643	0.427	0.866
0.311	1.3969	0.34	1.1685	0.35	0.9431	0.37	0.7672	0.3588	0.8753
0.23	1.4389	0.27	1.1965	0.28	0.955	0.304	0.7692	0.290	0.8817
0.15	1.469	0.20	1.2166	0.218	0.9627	0.238	0.7702	0.222	0.8856
0.07	1.487	0.13	1.2286	0.149	0.966	0.172	0.7706	0.154	0.8873
0	1.493	0.0625	1.2326	0.080	0.9675	0.106	0.7707	0.0859	0.8876
0	1.493	0.055	1.2326	0.071	0.9675	0.0948	0.07707	0.0764	0.8876
0	1.493	0.048	1.2325	0.062	0.9676	0.082	0.07707	0.0668	0.8876
0	1.493	0.041	1.2323	0.053	0.9677	0.071	0.7707	0.057	0.8876
0	1.493	0.034	1.232	0.044	0.9678	0.059	0.7708	0.0477	0.8877
0	1.493	0.027	1.2317	0.035	0.9677	0.047	0.7708	0.0382	0.8878
0	1.493	0.02	1.2312	0.026	0.9676	0.035	0.7709	0.02866	0.888
0	1.493	0.01	1.2307	0.017	0.9673	0.023	0.7709	0.019	0.8882
0	1.493	0.0069	1.2302	0.0089	0.967	0.01185	0.7710	0.0095	0.8887
0	1.493	0	1.2295	0	0.9666	0	0.7710	0	0.8895

parameter (θ_1) and electric field (U_e). Here the fact was verified that the Newtonian model possesses higher velocity when compared to the Casson (θ_2=1; θ_1= $2\sqrt{\theta_2\tau_0}$) and K-L fluid model (θ_2 = 0.1and1). Significantly, it is noted that the results based on the two-layered model share the same characteristics of the one-layer model concerned with the values of parameters considered. Moreover, the set of data points has been displayed in Table 4.

In Figure 7, the impact of the electric field and K-L parameter (θ_2) was interpreted in the velocity profiles. In the vicinity of the EDL effect, it had a high effect on the flow. The decreasing value of the electric field shows that velocity was reduced and the increasing value of θ_2 tends to reduce more. This shows that the K-L parameter (θ_2), can reduce the fluid flow. This is attributed to the fact that as the K-L parameter (θ_2) increases the apparent viscosity of the fluid slows down the motion of the fluid.

The distribution of velocity along the radial distance with the absence and the existence of an electric field is discussed in Figure 8. The variation of the K-L parameter and yield stress was studied and found that in the absence of an electric field, the higher the value of yield stress (τ_0) and θ_1 tends to slow down the velocity profiles whereas the existence of an electric field made a sudden upsurge in the fluid motion and the data sets have been displayed in Table 5.

Generally, the velocity of the fluid forms merely a parabolic form (depending on the fluid model). This shows that the velocity however higher at the midpoint, whereas it tends to be slower when it approaches the wall. This is because the fluid layer present at the wall made a friction effect with the layer of the wall. This sort of friction was caused due to the tangential force imposed by the fluid motion. This kind of friction is called Skin friction or wall shear stress. The rate at which fluid velocity increases as it travels from the conduit wall to the conduit's middle defines the magnitude of the wall shear stress.

In Figures 9-12, the wall shear stress was discussed with respect to the K-L parameters (θ_2). Here, the new findings have been analysed. Compared to the velocity profiles, the behaviour of K-L parameters(θ_2) and the Electric field projects its behaviour in the opposite nature. In Figure 9, the influence of the electric field is induced to reduce the wall shear stress whenever it increases. The required amount of friction force needed less because of the external electric field. Similarly, as the K-L parameter (θ_1) increases, the tendency of the friction force is also increased. Moreover, as the K-L parameter (θ_1) is held fixed, the magnitude of the skin friction is increased with the increase in (θ_2). Interestingly, the fact was found that the increasing nature of the K-L parameter (θ_2), tends to upsurge the magnitude of the skin friction. In wall shear stress, the Casson fluid

Table 4. Values for the velocity distribution along with radial direction for distinct values of yield stress (τ_0) and K-L parameter (θ_1) provided in Figure 6. [one-layered model with θ_2=1; $\theta_1 \le \theta_2$]

K-L-Newtonian (θ_1=1)		K-L-Newtonian (θ_1=0.1)		Casson-Newtonian		Bingham-Newtonian		Newtonian-Newtonian	
y-axis	**x-axis**	**y-axis**	**x-axis**	**y-axis**	**x-axis**	**y-axis**	**x-axis**	**y-axis**	**x-axis**
1	0.5	1	0.5	1	0.5	1	0.5	1	0.5
0.9012	0.525	0.8995	0.5812	0.8979	0.56	0.8958	0.6475	0.8889	0.7084
0.8025	0.5456	0.7989	0.6523	0.7958	0.6109	0.7917	0.7776	0.7778	0.8923
0.7037	0.5622	0.6984	0.7134	0.6937	0.653	0.6875	0.8903	0.6667	1.0517
0.6049	0.575	0.5979	0.7646	0.5915	0.6869	0.5834	0.9858	0.5556	1.1865
0.5062	0.5843	0.4974	0.8059	0.4894	0.7125	0.4792	1.0638	0.444	1.2969
0.4074	0.5905	0.3968	0.8375	0.3873	0.7305	0.3750	1.1246	0.333	1.3827
0.3086	0.5939	0.2963	0.8593	0.2852	0.7415	0.2709	1.1679	0.2222	1.444
0.2099	0.5954	0.1958	0.8717	0.1831	0.7466	0.1667	1.194	0.1111	1.4807
0.11	0.5956	0.0952	0.8753	0.081	0.7476	0.0625	1.2026	0	1.493
0.0988	0.5956	0.0847	0.8753	0.072	0.7476	0.0556	1.2026	0	1.493
0.0864	0.5956	0.0741	0.8751	0.063	0.7476	0.0486	1.2025	0	1.493
0.0741	0.5956	0.0635	0.8749	0.054	0.7476	0.0417	1.2023	0	1.493
0.0617	0.5957	0.0529	0.8745	0.045	0.7476	0.0347	1.2020	0	1.493
0.0494	0.5957	0.0423	0.8741	0.036	0.7477	0.0278	1.2017	0	1.493
0.037	0.5958	0.0317	0.8735	0.027	0.7478	0.0208	1.2012	0	1.493
0.0247	0.5959	0.0212	0.8728	0.018	0.7481	0.0139	1.2007	0	1.493
0.0123	0.5960	0.0106	0.8719	0.009	0.7484	0.0069	1.2002	0	1.493
0	0.5960	0	0.871	0	0.7489	0	1.1995	0	1.493

Table 5. Values of velocity distribution along with radial direction for distinct values of yield stress (τ_0), K-L parameter (θ_1) and Electric field (U_e) provided for Figure 8.

τ_0=0.1; θ_1=0.1; U_e=0		τ_0=0.1; θ_1=0.2; U_e=0		τ_0=0.1; θ_1=0.3; U_e=0		τ_0=0.2; θ_1=0.3; U_e=0		τ_0=0.2; θ_1=0.3; U_e=0.1	
y-axis	**x-axis**	**y-axis**	**x-axis**	**y-axis**	**x-axis**	**y-axis**	**x-axis**	**y-axis**	**x-axis**
1	0	1	0	1	0	1	0	1	0.1
0.96	0.0328	0.96	0.0328	0.96	0.0328	0.96	0.0328	0.96	0.1328
0.93	0.0644	0.93	0.0644	0.93	0.0644	0.93	0.0644	0.93	0.164
0.9	0.0950	0.9	0.095	0.9	0.095	0.9	0.095	0.9	0.1950
0.8667	0.1244	0.8667	0.1244	0.8667	0.1244	0.8667	0.1244	0.8667	0.2244
0.833	0.1528	0.833	0.1528	0.833	0.1528	0.833	0.1528	0.833	0.2528
0.8	0.18	0.8	0.18	0.8	0.18	0.8	0.18	0.8	0.28
0.7667	0.2061	0.7667	0.2061	0.7667	0.2061	0.7667	0.2061	0.7667	0.3061
0.733	0.2311	0.733	0.2311	0.733	0.2311	0.733	0.2311	0.733	0.3311
0.7	0.255	0.7	0.255	0.7	0.255	0.7	0.255	0.7	0.355
0.633	0.2881	0.633	0.2840	0.633	0.2804	0.644	0.2720	0.644	0.372
0.5667	0.3170	0.5667	0.3091	0.5667	0.3023	0.588	0.2866	0.588	0.3866
0.5	0.3418	0.5	0.3305	0.5	0.3207	0.533	0.2989	0.533	0.3989
0.43	0.3626	0.43	0.3481	0.43	0.3357	0.477	0.3088	0.477	0.4088
0.366	0.3792	0.366	0.362	0.366	0.3473	0.422	0.3165	0.422	0.4165
0.3	0.3919	0.3	0.3723	0.3	0.3558	0.3667	0.322	0.3667	0.422
0.233	0.4006	0.233	0.3792	0.233	0.3612	0.311	0.3256	0.311	0.4256
0.166	0.4055	0.166	0.3828	0.166	0.3639	0.2556	0.3273	0.2556	0.4273
0.1	0.4068	0.1	0.3836	0.1	0.3644	0.2	0.3276	0.2	0.4276
0.0889	0.4068	0.0889	0.3836	0.0889	0.3645	0.1778	0.3277	0.1778	0.4277
0.0778	0.4067	0.0778	0.3837	0.0778	0.3645	0.1556	0.328	0.1556	0.428
0.0667	0.4064	0.0667	0.3836	0.0667	0.3647	0.133	0.3277	0.133	0.4277
0.0556	0.4061	0.0556	0.384	0.0556	0.3648	0.11	0.3270	0.11	0.427
0.0444	0.4056	0.0444	0.383	0.0444	0.3647	0.0889	0.3258	0.0889	0.4258
0.0333	0.4049	0.0333	0.3826	0.0333	0.3645	0.0667	0.3241	0.0667	0.4241
0.0222	0.4042	0.0222	0.382	0.0222	0.3642	0.0444	0.3219	0.0444	0.4219
0.0111	0.4033	0.0111	0.3813	0.0111	0.3638	0.0222	0.3192	0.0222	0.4192
0	0.4023	0	0.3805	0	0.3633	0	0.316	0	0.416

along with the value of U_e=0 was 0.102 % approximately higher for U_e=0.5 and for the K-L model (U_e=0) is appropriately greater than 0.078 % for U_e=0.5. The one-layered and two-layered models were discussed graphically in the existence and absence of an electric field as seen in Figures 10-12. In Figure 10, Casson-Newtonian model ($\theta_1 = 2\sqrt{\theta_2 \tau_0}$) and the K-L- Newtonian model (θ_1) were made with relevant values. The Newtonian-Newtonian model and Bingham-Newtonian model are discussed in Figure 11. The Newtonian-Newtonian fluid has a lesser magnitude of skin friction than the Bingham-Newtonian fluid. The skin friction coefficient of the K-L-Newtonian model was higher friction than the Casson-Newtonian model. In both Figures 10 and 11, it is noticed that the electric field reduces the skin friction. Similarly, the characteristics analysed in Figure 12 are the one-layered model (K-L fluid and Casson fluid model) which shares the same behaviour exposed by the two-layered model. The comparison of the one-layer and two-layer models was analysed graphically and verified one-layered model features with the two-layered model.

In Figure 13, the interpretation of the pressure drop over the axial direction (z) was made. The prescribed model was designed with two additional body forces: pressure force and electro-osmotic force. Electric force always enhances fluid motion. If suppose this force is absent, the pressure force tends to play a vital role in making fluid flow. Owing to this fact, the concerned graph was studied. Scrutinizing the K-L parameters (θ_1&θ_2), the analysis of the pressure drop was discussed in Figure 13. It shows that the pressure drop exists only when $\theta_1 \leq \theta_2$ and the Δp increment is found for the increasing values of the K-L parameters. The pressure drop (Δ_p) for the K-L parameter θ_1=0.1, 0.2 is

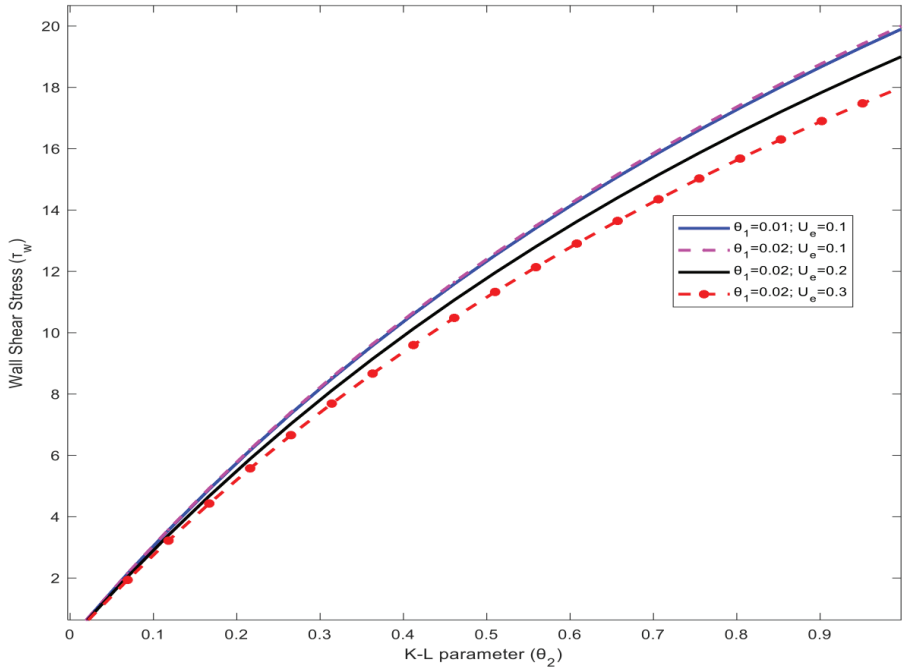

Figure 9. Variation of wall shear stress (τ_w) along with the K-L parameter (θ_2) for different values of K-L parameter (θ_1) and Electric field (U_e).

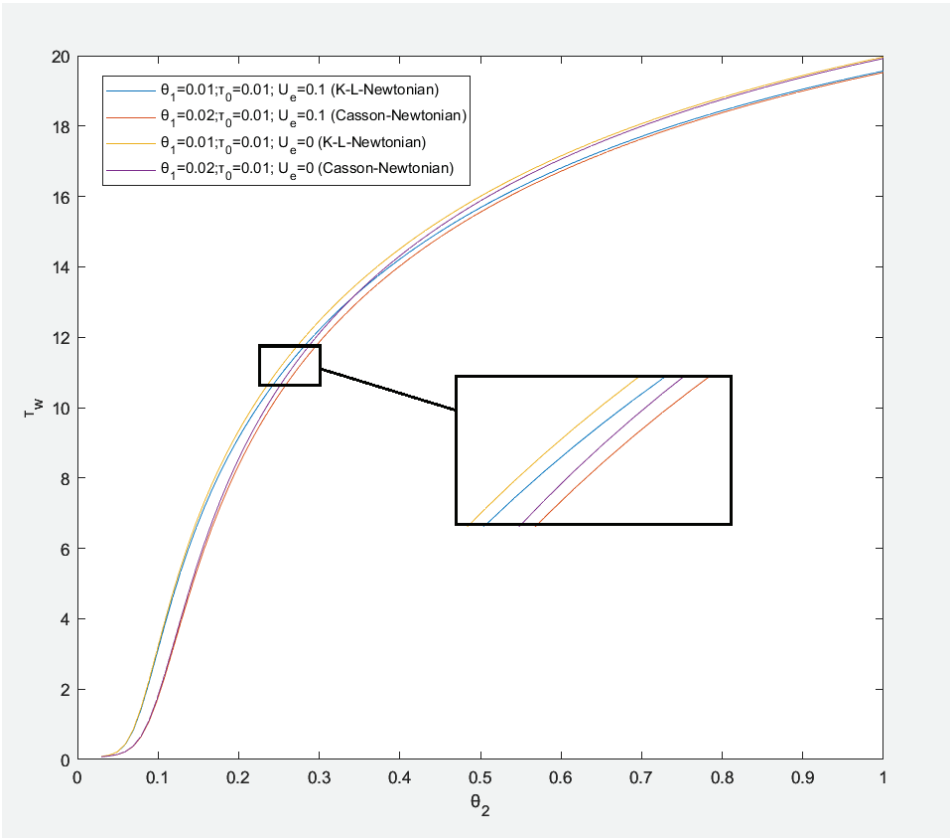

Figure 10. Variation of wall shear stress (τ_w) along with the K-L parameter (θ_2) for different values of K-L parameter (θ_1) and Electric field (U_e).

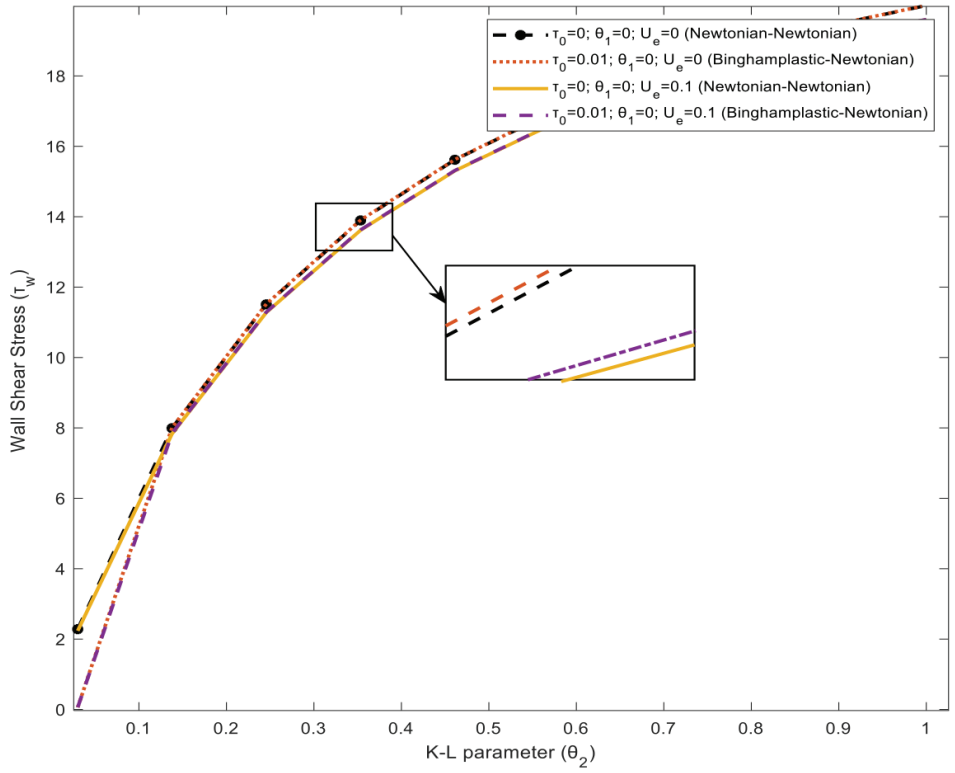

Figure 11. Variation of wall shear stress (τ_w) along with the K-L parameter (θ_2) for different values of K-L parameter (θ_1) and Electric field (U_e).

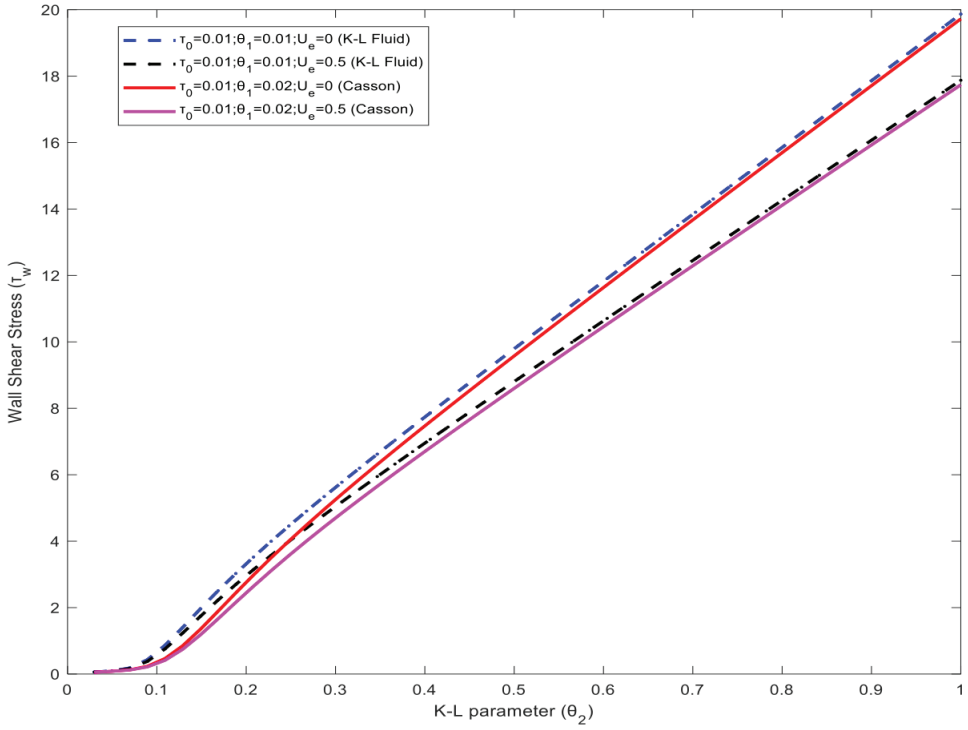

Figure 12. Variation of wall shear stress (τ_w) along with the K-L parameter (θ_2) for different values of K-L parameter (θ_1) and Electric field (U_e) for one-layered model.

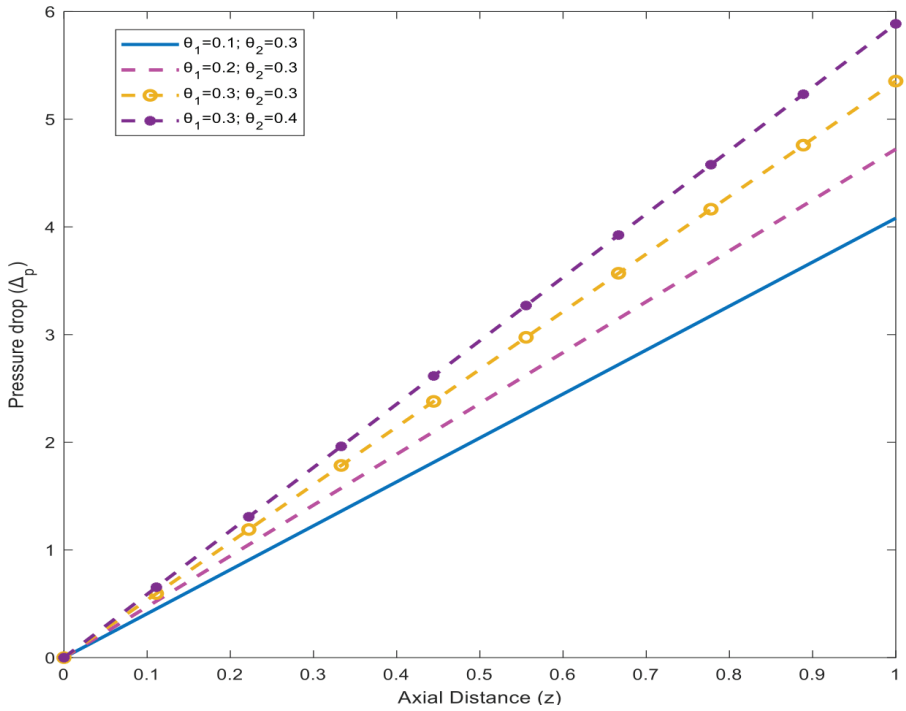

Figure 13. Variation of pressure drop (Δp) along with the axial direction (z) for different values of K-L parameters (θ_1& θ_2).

Table 6. Values for the variation of pressure drop (Δp) along with the axial direction (z) for different values of K-L parameters (θ_1& θ_2) provided in Figure 13.

θ_1=0.3; θ_2=0.4		θ_1=0.3; θ_2=0.3		θ_1=0.2; θ_2=0.3		θ_1=0.1; θ_2=0.3	
x-axis (z)	**y-axis (Δ_p)**	**x-axis (z)**	**y-axis (Δ_p)**	**x-axis (z)**	**y-axis (Δ_p)**	**x-axis (z)**	**y-axis (Δ_p)**
0	0	0	0	0	0	0	0
0.1	0.654	0.1	0.5949	0.1	0.5247	0.1	.4535
0.2	1.308	0.2	1.1898	0.2	1.0493	0.2	.9069
0.3	1.962	0.3	1.7847	0.3	1.574	0.3	1.3604
0.4	2.616	0.4	2.3797	0.4	2.0986	0.4	1.8138
0.5	3.27	0.5	2.9746	0.5	2.6233	0.5	2.2673
0.6	3.924	0.6	3.5695	0.6	3.1479	0.6	2.7207
0.7	4.578	0.7	4.1644	0.7	3.6726	0.7	3.1742
0.8	5.232	0.8	4.7593	0.8	4.1972	0.8	3.6276
1	5.886	1	5.342	1	4.7219	1	4.0811

approximately 0.21 % higher than the θ_1=0.3 for the fixed viscosity index θ_2=0.3 and the set of data points has been displayed in Table 6.

In Figures 14 and 15, the impact of the yield stress over the plug core radius region was computed numerically. Depending on the various factors, the analysis was done. The plug core radius is dependent on the pressure gradient and the yield stress of the given fluid model. Plug core radius possesses a visco-plastic nature and the velocity of the fluid in this section is almost constant. This proves that the growth of the radius in the plug core area is linear with respect to the yield stress. Owing to this fact, the assumed parameters are K-L parameters, Constant interfacial region and electric field. The variation of the Interfacial region and the electric field was discussed in Figure 14. The potential of the electric field has a tendency to make the fluid region move forward and its enhancement has occurred in a small amount. Furthermore, the interfacial region also plays a vital role in the plug core region. It validates the increasing volume of core fluid radius (i.e., interfacial radius), and its influence

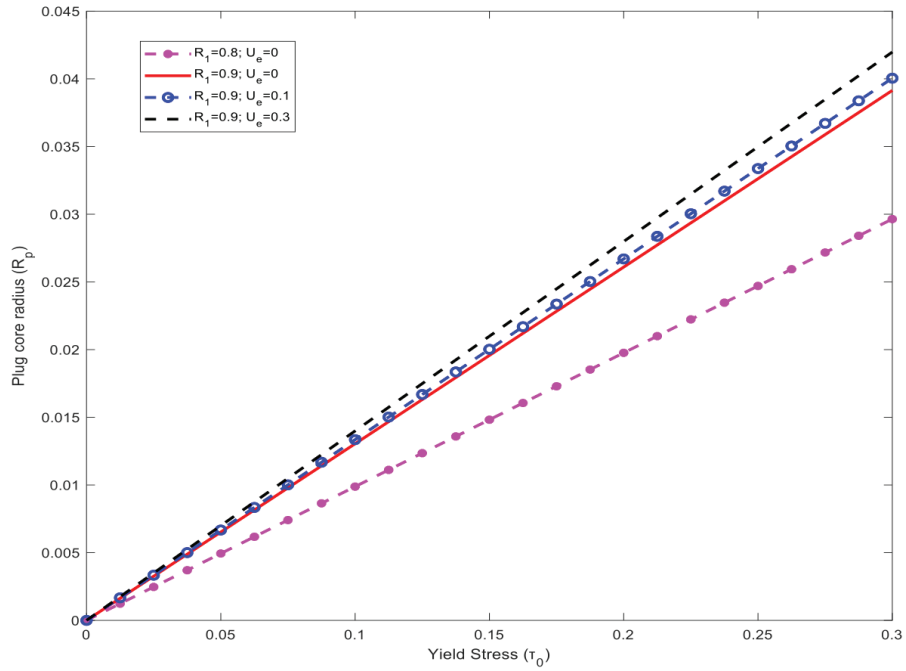

Figure 14. Variation of plug core radius (R_p) along with yield stress (τ_0) for different values of interfacial Region (R_1) and Electric field (U_e).

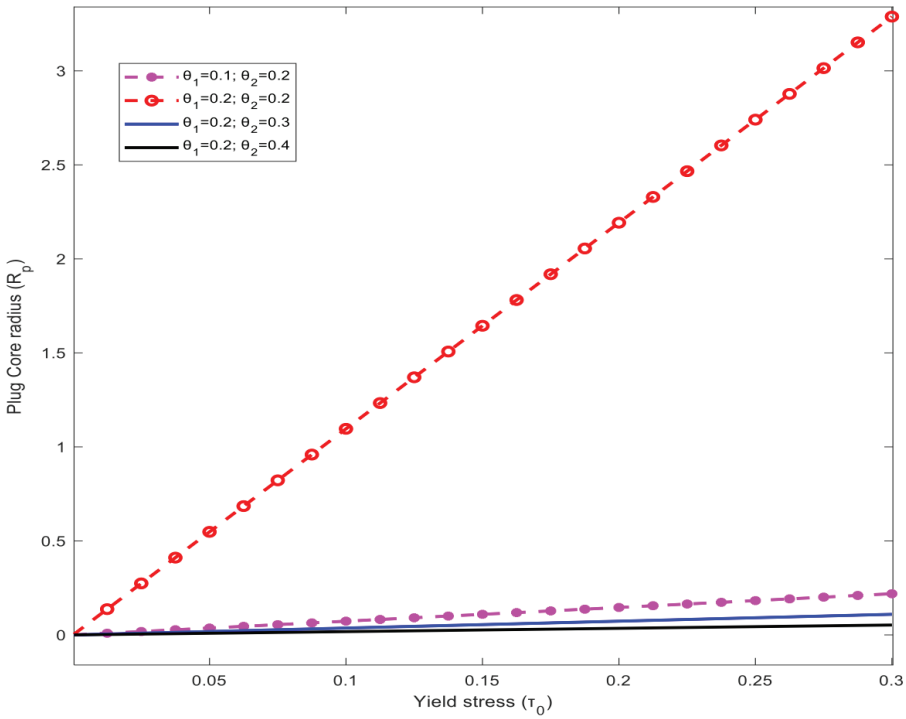

Figure 15. Variation of plug core radius (R_p) along with yield stress (τ_0) for different values of K-L parameters (θ_1 & θ_2).

causes the increase in the region in the plug flow region. In Figure 15, the variation of the K-L parameters (θ_1, θ_2) was interpreted with appropriate values. The influence of the K-L parameter θ_1 was higher than the θ_2. The enhancement of the θ_2 value suppresses the plug core radius and the opposite behaviour was identified in the θ_1 parameter.

The variation of the flow flux was discussed in Figures 16-18 with respect K-L parameter (θ_2). In Figure 16, we

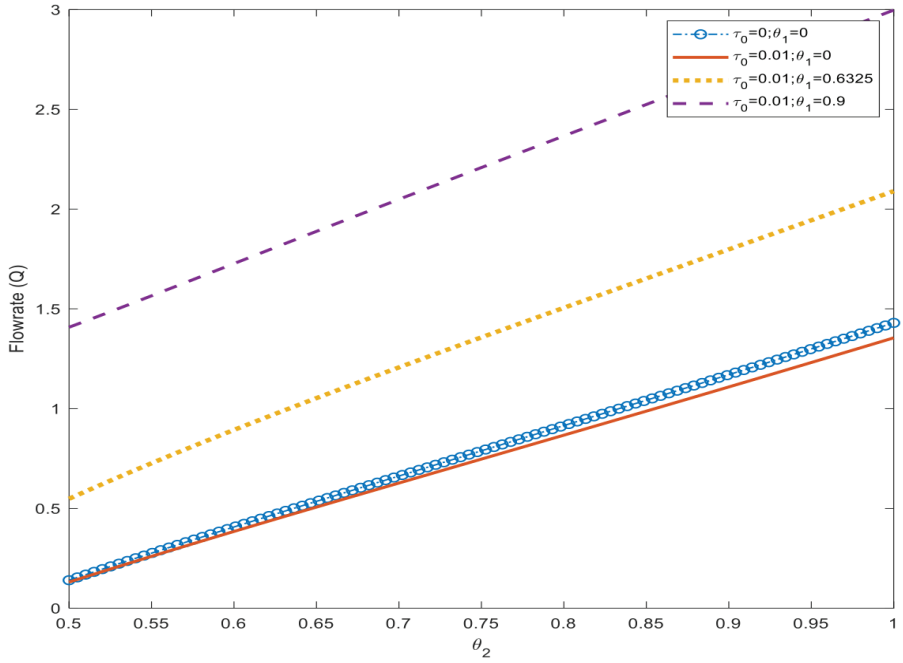

Figure 16. Variation of flow rate with respect to the K-L parameter (θ_2) for the distinct values of yield stress (τ_0) and K-L parameter (θ_1).

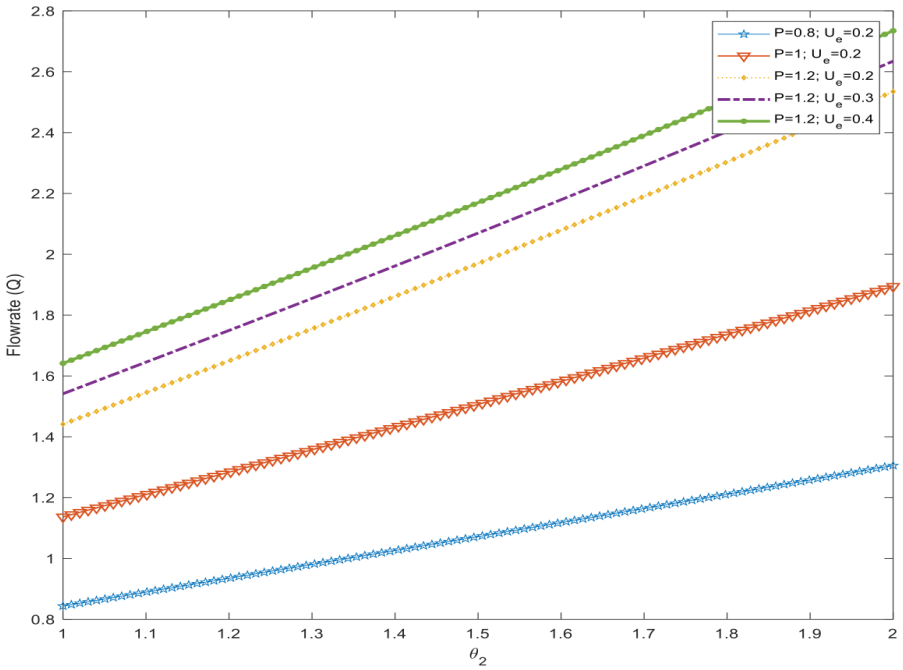

Figure 17. Variation of flow rate with respect to the K-L parameter (θ_2) for the distinct values of pressure gradient (P) and Electric field (U_e).

analysed the variation of flow rate for the distinct values of yield stress (τ_0) and K-L parameter (θ_1). Here, the observation was made that the flow rate was diminished for the increment value of yield stress. This is due to the fact that the component yield stress represents the solid behaviour of the fluid. If the fluid accumulates the yield stress component, the extra additional force is required to make a fluid move in the conduit. Owing to this physiological fact,

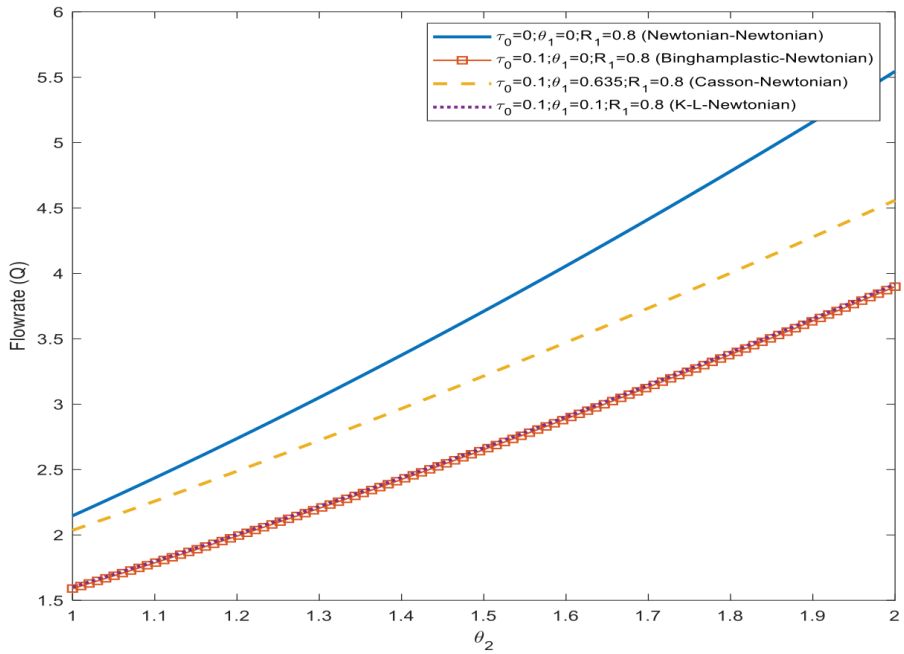

Figure 18. Variation of flow rate with respect to the K-L parameter (θ_2) for the different types of fluids in limiting cases.

our model portrayed these behaviours very well. For the enhanced values of the K-L parameter (θ_1), the flow rate was increased which shows that the component θ_1 provides the favourable quality to ingrown the motion of the flux. The variation of the flow flux was studied for the distinct values of pressure gradient and the electroosmotic flow in Figure 17. This figure shows that the enhancement of flow flux occurs for the increasing values of the pressure gradient and the electroosmotic force. Figure 18 portrays the flow rate of different kinds of fluids with respect to the K-L parameter (θ_2) with certain limiting cases. It shows that Newtonian-Newtonian fluids possess high flow flux compared to the Bingham plastic-Newtonian, Casson-Newtonian and K-L-Newtonian. This is due to the fact that the presence of yield stress makes the fluid decrease its flow wherever it exists and the corresponding data sets for this respective figure are shown in Table 7 to indicate the values of each kind of fluid flow.

Table 7. Variation of flow rate with respect to the K-L parameter (θ_2) for the different types of fluids in limiting cases in Figure 18.

Newtonian-Newtonian		Bingham Plastic-Newtonian		Casson - Newtonian		K-L - Newtonian	
x-axis	y-axis	x-axis	y-axis	x-axis	y-axis	x-axis	y-axis
1.0000	1.0410	1.0000	0.6040	1.0000	0.9480	1.0000	0.6137
1.0714	1.1720	1.0714	0.6710	1.0714	1.0300	1.0714	0.6808
1.1428	1.3040	1.1428	0.7380	1.1428	1.1110	1.1428	0.7483
1.2142	1.4380	1.2142	0.8050	1.2142	1.1930	1.2142	0.8164
1.2857	1.5750	1.2857	0.8740	1.2857	1.2740	1.2857	0.8852
1.3571	1.7140	1.3571	0.9430	1.3571	1.3560	1.3571	0.9549
1.4285	1.8540	1.4285	1.0130	1.4285	1.4390	1.4285	1.0255
1.5000	1.9980	1.5000	1.0850	1.5000	1.5220	1.5000	1.0970
1.5714	2.1430	1.5714	1.1570	1.5714	1.6050	1.5714	1.1690
1.6428	2.2920	1.6428	1.2300	1.6428	1.6900	1.6428	1.2430
1.7142	2.4420	1.7142	1.3050	1.7142	1.7750	1.7142	1.3180
1.7857	2.5950	1.7857	1.3800	1.7857	1.8620	1.7857	1.3940
1.8571	2.7510	1.8571	1.4570	1.8571	1.9490	1.8571	1.4710
1.9285	2.9090	1.9285	1.5350	1.9285	2.0370	1.9285	1.5490
2.0000	3.0700	2.0000	1.6140	2.0000	2.1264	2.0000	1.6280

Table 8. Rheological parameter values. [From Manchi and Ponalagusamy [38], with permission from Elsevier]

H (%)	R_1 (cm)	τ_0^* (dyne/cm^2)	η_1^* (dyne-s$^{1/2}$/ cm^2)	η_2^* (dyne-s$^{1/2}$/ cm^2)
20	0.84	0.00201	0.01871	0.02912
30	0.85	0.00593	0.03790	0.03102
40	0.86	0.02383	0.08406	0.04026

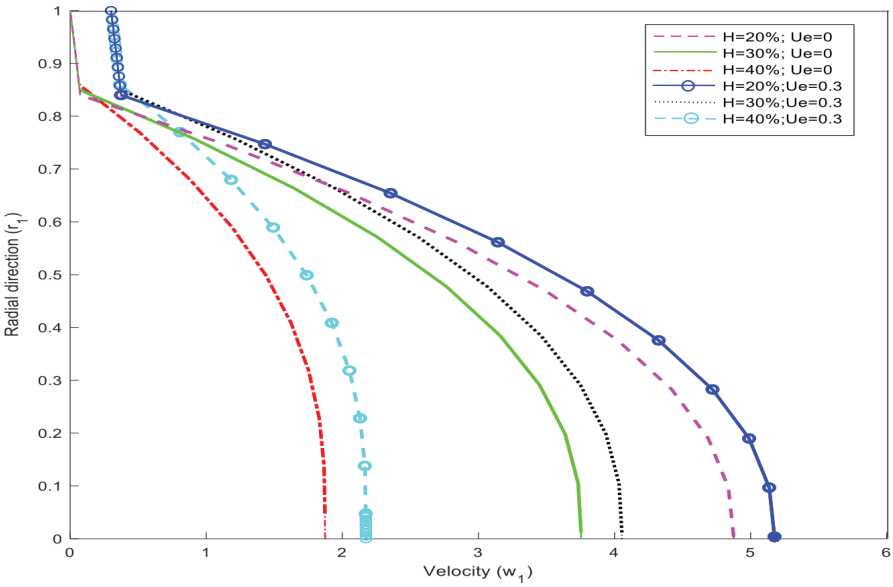

Figure 19. Velocity distribution along with radial direction for distinct values of hematocrit in the presence and absence of an electric field through a rigid tube.

Real-Life Application

The present formulation gives an effective way of studying the K-L- Newtonian fluid model under the impact of an electric field. So far, the application of the concern fluid model has been utilized in the form of blood transport in normal and stenosed arteries. Here, we gave the flow behaviour of common rheology of the immiscible fluids under the impact of the electric field. Moreover, the fluid becomes very effective when the concentration of the suspended particles (maybe nano-particles in fluids or red blood cells in blood flow) in immiscible fluids can be discussed. Inspired by the human blood model, the present model sheds some limelight to make engineering-based applications.

Table 8 provides the experimental values of hematocrit, K-L parameter and yield stress in dimensional form. In addition to that, appropriate values were used and the discussion was made about the existence and absence of an electric field. This exhibits that the velocity decreases with the increasing value of hematocrit. Moreover, the electric field possesses some additional force to enhance the velocity as displayed in Figure 19. This simulation technique will foresight its application in high polymer structure fluids. For instance, silver conductive grease, copper conductive grease, carbon nanotube conductive grease and graphite conductive grease are electrically conductive. Based on the percentage of silver, copper, graphite and carbon nanotube present in the concerned lubricants is similar to the hematocrit in blood. Depending on these percentages, the motion of the fluid and its resistance can be calculated. These electrically conductive lubricants (presence of additive) will be applicable in connectors and slip rings, switches and potentiometers, printed circuit boards, semiconductor devices, automotive applications, aerospace technology and Defence sectors. The aforementioned idea will spark the production of suitable fluid applications in the engineering industry.

CONCLUSION

The motion of immiscible fluids in the circular tube constrained by the external electric field was discussed. The fluid confined in the core section is Kuang-Luo (K-L) fluid which is surrounded by another fluid occupied in the outer

region the Newtonian fluid. It is presumed that both fluids are electrically conducting fluids. In addition to pressure force, the electric field tends to create an electroosmotic force and forms an EDL effect near the conduit wall. Based on this consideration, studies on the velocity profiles, wall shear stress, plug core radius and pressure drop were made and the following results were obtained.

- In the velocity profiles, yield stress, K-L parameters, intermediate thickness, and electric fields were discussed, and the augmentation of velocity was found when the electric field increased and the depletion of motion occurred when K-L parameters and yield stress were increased.
- The results obtained for the one-layered model possess a similar behaviour to the two-layer model, but they noticed that the velocity of the two-layer model is much higher than the one-layer model. This is due to the interfacial effects of the fluids.
- The depletion nature of the velocity was spotted in the increasing hematocrit value, and its behaviour was similar in the presence and absence of electric potential distribution.
- In the wall shear stress, the nature of the behaviour of the K-L parameter(θ_2) and the electric field was opposite when compared to the velocity profiles. The impact of K-L parameters (θ_1&θ_2) makes the wall shear stress increase and the enhancement of the electric field makes the wall shear stress decrease.
- The analysis of the pressure drop was discussed over the K-L parameters (θ_1 & θ_2). It shows the increasing effects of the pressure drop caused by the K-L parameter (θ_1 & θ_2).
- The interpretation of plug core radius with corresponding yield stress was discussed under the variation of K-L parameters, electric field, and interfacial region, and the concern effects were noted. The augmentation of plug core radius occurs for increasing values of the electric field, interfacial thickness, and θ1, and the opposite nature is shown in θ_2.
- For the first time, it is reported that for any value of the yield stress, the flow of two-phase immiscible fluids exhibits a realistic flow phenomenon when $\theta_1 \leq \theta_2$.
- A significant amount of declined percentage has been noticed in the two-layered Newtonian-Newtonian model which is approximately higher than the Casson-Newtonian (6.74%), Bingham-Newtonian (17.92%) and K-L-Newtonian (22.77%) in velocity profiles.
- In the case of wall shear stress, the value of Casson fluid for Ue=0 is approximately 1.02% higher for U_e=0.5 and similarly, the K-L model (U_e=0) is approximately 0.078 % greater for U_e=0.5.
- The pressure drop (Δp) for the K-L parameter θ_1=0.1, 0.2 is approximately 0.21 % higher than the θ_1=0.3 for the fixed viscosity index θ_2=0.3.
- The flow flux was enhanced for the increased values of pressure gradient, electroosmotic force and θ_1 and the opposite trend was observed for the higher values of yield stress.

Hence, the present work sheds some light on the outcome of the K-L Newtonian model under the impact of an electric field and on the varying nature of yield stress, K-L parameters, and peripheral thickness. This model can be further extended to various environments, like the existence of a magnetic field, by inducing nanoparticles and the conduit that possesses the peristaltic behaviour.

ACKNOWLEDGEMENTS

The corresponding author (Ms Sangeetha J) is grateful to the Ministry of Human Resource Development (MHRD), the Government of India for the grant of a research fellowship.

AUTHORSHIP CONTRIBUTIONS

Authors equally contributed to this work.

DATA AVAILABILITY STATEMENT

The requisite data used for numerical simulations and comparison purposes are evaluated using the aid of MATLAB software and demonstrated graphically.

CONFLICT OF INTEREST

The author declared no potential conflicts of interest with respect to the research, authorship, and/or publication of this article.

ETHICS

There are no ethical issues with the publication of this manuscript.

NOMENCLATURE

Alphabets

w_{11}, w_{12}	Velocity in core and peripheral region.
w_{pc}	Plug core velocity
p_0	Pressure
r_1, z_1	radial and axial direction
$-\frac{dp_0}{dz_1}$	Pressure gradient
R_1	Interfacial radius
R_{pc}	Plug core radius
U_e	Electrokinetic slip velocity
Q	Flow flux

Greek Symbols

$\tau_{r_1 z_1}$	Shear stress in $r_1 z_1$ plane
θ_1 & θ_2	K-L parameters
ε	Permittivity of the fluid
μ_n	viscosity of the Newtonian fluid

τ_0	yield stress
ρ_e	net charge density
τ_w	wall shear stress
Δp	pressure drop

REFERENCES

[1] Bentwich M. Two-phase viscous axial flow in a pipe. J Basic Eng 1964;86:669–672. [CrossRef]

[2] Packham BA, Shail R. Stratified laminar flow of two immiscible fluids. Proc Camb Philos Soc 1971;69:443–448. [CrossRef]

[3] Chaturani P, Ponalgusamy R. A two layered model for blood flow through stenosed arteries. Proc 11th Natl Conf Fluid Mech Fluid Power 1982:16–22.

[4] Vijayaraghavan Srinivasan, Vafai K. Analysis of linear encroachment in two-immiscible fluid systems in a porous medium. J Basic Eng 1994;116:135–139. [CrossRef]

[5] Chamkha AJ. Flow of two-immiscible fluids in porous and nonporous channels. J Fluids Eng 2000;122:117–124. [CrossRef]

[6] Umavathi JC, Chamkha AJ, Mateen A, Al-Mudhaf A. Unsteady two-fluid flow and heat transfer in a horizontal channel. Heat Mass Transf 2005;42:81–90. [CrossRef]

[7] Umavathi JC, Prathap Kumar J, Shekar M. Mixed convective flow of immiscible viscous fluids confined between a long vertical wavy wall and a parallel flat wall. Int J Eng Sci Technol 2010;2:256–277. [CrossRef]

[8] Prathap Kumar J, Umavathi JC, Chamkha AJ, Pop I. Fully-developed free-convective flow of micropolar and viscous fluids in a vertical channel. Appl Math Model 2010;34:1175–1186. [CrossRef]

[9] Ponalagusamy R, Tamil Selvi R. Brief communications: Two-layered model (Casson-Newtonian) for blood flow through an arterial stenosis with axially variable slip velocity at the wall. Int J Eng Sci Adv Comput Biotechnol 2013;4:71–74.

[10] Umavathi JC, Shekar M. Mixed convective flow of immiscible fluids in a vertical corrugated channel with traveling thermal waves. J King Saud Univ Eng Sci 2014;26:49–68. [CrossRef]

[11] Devakar M, Ramgopal NCh. Fully developed flows of two immiscible couple stress and Newtonian fluids through nonporous and porous medium in a horizontal cylinder. J Porous Media 2015;18:549–558. [CrossRef]

[12] Yadav PK, Verma AK. Analysis of immiscible Newtonian and non-Newtonian micropolar fluid flow through porous cylindrical pipe enclosing a cavity. Eur Phys J Plus 2020;135:645. [CrossRef]

[13] Akbari S, Taghavi SM. Buoyant fluid injections at high viscosity contrasts in an inclined closed-end pipe. Phys Fluids 2023;35:022102. [CrossRef]

[14] Houston G, Oliveria MSN. Flow focusing with miscible fluids in microfluidic devices. Phys Fluids 2023;35:052015. [CrossRef]

[15] Ponalagusamy R. Analysis of MHD flow of blood in stenosed arteries with radially variable viscosity and peripheral plasma layer thickness by means of Frobenius method. ESS Open Arch 2023:1–21.

[16] Rao AR, Usha S. Peristaltic transport of two immiscible viscous fluids in a circular tube. J Fluid Mech 1995;298:271–285. [CrossRef]

[17] Vajravelu K, Arunachalam PV, Sreenadh S. Unsteady flow of two immiscible conducting fluids between two permeable beds. J Math Anal Appl 1995;196:1105–1116. [CrossRef]

[18] Umavathi JC, Shekar M. Mixed convective flow of immiscible fluids in a vertical corrugated channel with traveling thermal waves. J King Saud Univ Eng Sci 2014;26:49–68. [CrossRef]

[19] Nikodijević DD, Stamenković ŽM, Jovanović MM, Kocić MM, Nikodijević JD. Flow and heat transfer of three immiscible fluids in the presence of uniform magnetic field. Therm Sci 2014;18:1019–1028. [CrossRef]

[20] Fraggedakis D, Kouris C, Dimakopoulos Y, Tsamopoulos J. Flow of two immiscible fluids in a periodically constricted tube: transitions to stratified, segmented, churn, spray, or segregated flow. Phys Fluids 2015;27:082102. [CrossRef]

[21] Abd Elmaboud Y. Two layers of immiscible fluids in a vertical semi-corrugated channel with heat transfer: impact of nanoparticles. Results Phys 2018;9:1643–1655. [CrossRef]

[22] Devakar M, Ramgopal NCh. Fully developed flows of two immiscible couple stress and Newtonian fluids through nonporous and porous medium in a horizontal cylinder. J Porous Media 2015;18:549–558. [CrossRef]

[23] Devakar M, Raje A. Modelling and analysis of the unsteady flow and heat transfer of immiscible micropolar and Newtonian fluids through a pipe of circular cross section. J Braz Soc Mech Sci Eng 2018;40:1–18. [CrossRef]

[24] Hue SH, Chagot L, Angeli P. Viscoelastic effects of immiscible liquid-liquid displacement in microchannels with bends. Phys Fluids 2022;34:073111. [CrossRef]

[25] Fang S, Zhenhua C, Baochang S, Meng Z. Optimal displacement of immiscible two-phase fluids in a pore doublet. Phys Fluids 2023;35:053332. [CrossRef]

[26] Sangeetha J, Ponalagusamy R. Impacts of electromagnetic and porous medium on time-dependent flow of two immiscible fluids in a channel. AIP Conf Proc 2023;2875:020003:1–11. [CrossRef]

[27] Akbari N, Gholinia M, Gholinia S, Dabbaghian S, Javadi H, Ganji DD. Analytical and numerical study of micropolar fluid flow in a porous plate due to linear stretching. Sigma J Eng Nat Sci 2018;36:1181–1196.

[28] Gholinia M, Javadi H, Gatabi A, Khodabakhshi A, Ganji DD. Analytical study of a two-phase revolving system of nanofluid flow in the presence of a magnetic field to improve heat transfer. Sigma J Eng Nat Sci 2019;37:341–360.

[29] Gholinia M, Gholinia S, Javadi H, Ganji DD. Investigation of micropolar fluid flow and heat transfer in a two dimensional permeable channel by analytical and numerical method. Sigma J Eng Nat Sci 2019;37:393–413.

[30] Dewangan SK, Senapati SK, Deshmukh V. CFD prediction of oil-water two phase stratified flow in a horizontal channel coupled level set-VOF approach. Sigma J Eng Nat Sci 2020;38:1–19.

[31] Özkan R, Ergüner A, Koca K, Genç MS. Improvement of mechanical behaviour of wind turbine blade using nanofluid-graphene and/or glass fiber in epoxy resin. Sigma J Eng Nat Sci 2021;39:58–69.

[32] Akaje TW, Olajuwon BI, Raji MT. Computational analysis of the heat and mass transfer in a Casson nanofluid with variable inclined magnetic field. Sigma J Eng Nat Sci 2023;41:512–523. [CrossRef]

[33] EL Hattab M, Boumhaout M, Oukach S. MHD natural convection in a square enclosure using carbon nanotube-water nanofluid with two isothermal fins. Sigma J Eng Nat Sci 2024;42:1075–1087. [CrossRef]

[34] Luo XY, Kuang ZB. A study on the constitutive equation of blood. J Biomech 1992;25:959. [CrossRef]

[35] Zhang JB, Kuang ZB. Study on blood constitutive parameter in different blood constitutive equations. J Biomech 2000;33:355–360. [CrossRef]

[36] Sriyab S. Mathematical analysis of non-newtonian blood flow in stenosis narrow arteries. Comput Math Methods Med 2014;2014:479152:1–10. [CrossRef]

[37] Bali R, Gupta N. Study of non-newtonian fluid by K–L model through a non-symmetrical stenosed narrow artery. Appl Math Comput 2018;320:358–370. [CrossRef]

[38] Ponalagusamy R, Machi R. A study on two-layered (K-L-Newtonian) model of blood flow in an artery with six types of mild stenoses. Appl Math Comput 2020;367:1–22. [CrossRef]

[39] Ponalagusamy R, Machi R. Mathematical study on two-fluid model for flow of K-L fluid in a stenosed artery with porous wall. SN Appl Sci 2021;3:508. [CrossRef]

[40] Ponalagusamy R, Machi R. Biorheological model on pulsatile flow of blood (K–L fluid) through flexible stenotic tapered blood vessels. Int J Appl Comput Math 2021;7:1–13. [CrossRef]

[41] Singh S, Murthy PVSN. Unsteady dispersion in pulsatile Luo and Kuang blood flow (K-L model) in a tube with wall reactive absorption. J Non Newtonian Fluid Mech 2022;310:104928. [CrossRef]

[42] Ponalagusamy R, Murugan D, Tamil Selvi R. Effects of rheology of non-newtonian fluid and chemical reaction on a dispersion of a solute and implications to blood flow. Int J Appl Comput Math 2022;8:109. [CrossRef]

[43] Gao Y, Wong TN, Yang C, Ooi KT. Two-fluid electroosmotic flow in microchannels. J Colloid Interface Sci 2005;284:306–341. [CrossRef]

[44] Zhao C, Yang C. Electrokinetic of non-newtonian fluids: A review. Adv Colloid Interface Sci 2013;201–202:94–108. [CrossRef]

[45] Afonso AM, Alves MA, Pinbo FT. Analytical solution of two-fluid electro-osmotic flows of viscoelastic fluids. J Colloid Interface Sci 2013;395:277–286. [CrossRef]

[46] Goswami P, Chakraborty J, Bandobadhyay A, Chakraborty S. Electrokinetically modulated peristaltic transport of power-law fluids. Microvasc Res 2016;103:41–54. [CrossRef]

[47] Gaikwad H, Basu DN, Mondal PK. Electroosmotic transport of immiscible binary system with a layer of non-conducting fluid under interfacial slip: The role applied pressure gradient. Electrophoresis 2016;37:1998–2009. [CrossRef]

[48] Chaube MK, Yadav A, Tripathi D, Bég AO. Electroosmotic flow of biorheological micropolar fluids through microfluidic channels. Korea Aust Rheol J 2018;30:89–98. [CrossRef]

[49] Ali N, Hussain S, Ullah K, Bég AO. Mathematical modelling of two fluid electroosmotic peristaltic pumping an Ellis fluid in an axisymmetric tube. Eur Phys J Plus 2019;134:1–18. [CrossRef]

[50] Hussain S, Ali N. Electro-kinetically modulated peristaltic transport of multilayered power-law fluid in an axisymmetric tube. Eur Phys J Plus 2020;135:1–24. [CrossRef]

[51] Ponalagusamy R, Sangeetha J. A study on electro-hydrodynamic flow of two immiscible fluids in a circular tube. Proc 66th Congr ISTAM Int Conf 2021.

[52] Mukherjee S, Shit GC, Vajravelu K. Effects of diffusive Reynolds number on electro-osmotic pulsating nanofluid flow. Phys Fluids 2022;34:122004. [CrossRef]

[53] Kahali T, Santra S, Chakraborty S. Electrically modulated cross-stream migration of a compound drop in micro-confined oscillatory flow. Phys Fluids 2022;34:122015. [CrossRef]

[54] Ismayeel M, Mehta SK, Mondal PK. Prediction of electrodiffusio-osmotic transport of shear thinning fluids in a nanochannel using artificial neural network. Phys Fluids 2023;35:012018. [CrossRef]

[55] Ponalagusamy R, Sangeetha J. Electroosmotic effect on two immiscible (conducting–non-conducting) fluids flowing in the porous channel under magnetic field. Proc IMechE Part E J Process Mech Eng 2023;237:2029–2044. [CrossRef]

[56] Sangeetha J, Ponalagusamy R, Tamil Selvi R. Unsteady peristaltic flow of two immiscible fluids in an elastic tube under the effect of electromagnetic force and outer region with the porous medium. Proc 68th Congr Indian Soc Theor Appl Mech Int Conf 2023.

[57] Sangeetha J, Ponalagusamy R, Tamil Selvi R. Electroosmotic peristaltic flow of thixotropic-Newtonian fluids in a circular tube: Effect of variable viscosity co-efficient of core fluid. Chin J Phys 2024;92:470–493. [CrossRef]